

**Computational Studies of Mitragynine Analogue Binding at  
the Human Mu-Opioid Receptor**

Undergraduate Honors Research Thesis

Presented in partial fulfillment of the requirements for graduation with  
honors research distinction in the undergraduate colleges of The Ohio  
State University

by

James E. Fanning

The Ohio State University

May 2020

Project Advisors: Dr. Noel M. Paul & Dr. Richard Spinney, Department  
of Chemistry and Biochemistry

## **Abstract**

The mu-opioid receptor (MOR) is a well-characterized G-protein coupled receptor and a major target of opioid pharmaceuticals. Opioid agonists exert their effects by MOR binding through two major downstream pathways: G-protein signaling and beta-arrestin signaling. The design of MOR agonists that favor or exclusively activate G-protein signaling may provide a new class of pharmaceuticals for pain relief with improved side-effect profiles. Mitragynine is the active compound of the herbal supplement kratom. Its distinct molecular structure and potential G-protein bias has gained increasing attention. Mitragynine analogues were designed and tested in-silico using several computer-aided drug design approaches. A homology model of the human MOR was constructed in Swiss-Model using a murine MOR crystal structure (PDB: 5C1M). A compound library of mitragynine analogues was iteratively constructed and passed through the SwissADME web tool to predict pharmacokinetics before molecular docking. Analogues with predicted access to the central nervous system (CNS) underwent water-solvent geometry optimization in Spartan and were simulated in the human MOR active site by a flexible ligand-rigid receptor docking calculation in AutoDock Vina. Analogues with MOR-activity comparable to mitragynine were retained for simulation in a flexible ligand-flexible receptor calculation for improved accuracy. Notably, results revealed several CNS-accessible analogues with similar in-silico activity at the human MOR compared to existing biased and mitragynine-analogue agonists. This computational study provides direction for the rational drug design of mitragynine toward G-protein biased agonists by identifying several analogues with potential activity at the human MOR. These findings prompt follow-up pharmacological testing to establish if these lead compounds act as agonists and possess a bias for G-protein signaling.

## Acknowledgements

My first acknowledgements are to my research advisors for this project, Dr. Noel M. Paul and Dr. Richard Spinney. Dr. Paul renewed my interests in biochemistry and pharmacology through his Chemistry 5230 course and took me on when I approached him about the prospect of a thesis in chemistry. I thank Dr. Spinney for introducing me to computational chemistry and protein modeling, providing me with the skills to design and execute this project. Your courses, expertise, and mentorship have molded me into a better scientist. Coordinating my work for this project between both of you was a highlight of my senior year.

I must also give thanks to my research advisor within microbiology, Dr. Birgit Alber. Dr. Alber first fascinated me with the molecular mechanisms of action in light-energy capturing reactions. Dr. Alber would later enable me to utilize the computational and chemical skillsets learned for this project in her own laboratory towards an independent study.

To Dr. Christopher M. Hadad, thank you for serving on the defense committee. Dr. Hadad gave a presentation of his research to the Chemistry 5230 course which first exposed me to computational research, particularly homology modeling and docking. His presentation first turned the gears in my mind that drove me to computational research for its power and autonomy.

Thank you to all of the professors in my humanities and sciences courses who molded me into the student and scientist that I am today; to the Honors and Scholars Department for awarding me a scholarship towards this thesis; and to The Ohio State University Department of Chemistry and Biochemistry for laboratory access and enabling a non-chemistry major to still pose a question within their field.

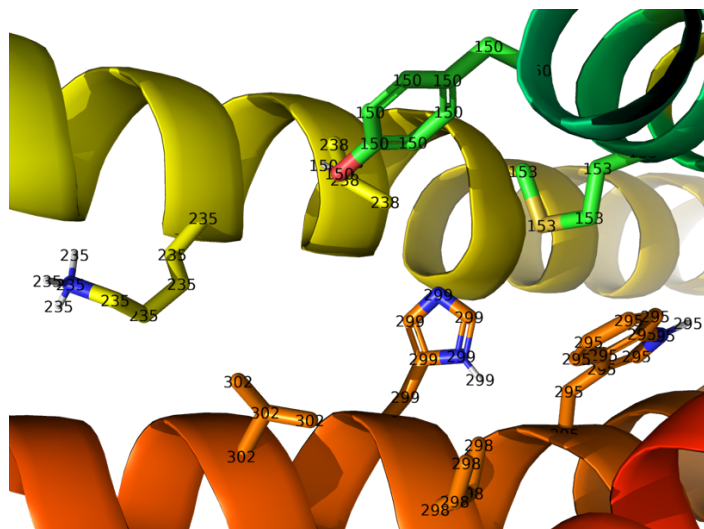
## Table of Contents

Abstract.....	i
Acknowledgements.....	ii
I. Introduction.....	1
II. Methodology.....	4
A. Human Mu-Opioid Receptor Homology Modeling.....	4
B. In-Silico Exploration of Activity in Six Mu-Opioid Receptor Biased Agonists.....	4
<i>Geometry Optimizations.....</i>	<i>4</i>
<i>Preparation for AutoDock Vina Docking.....</i>	<i>4</i>
<i>7-OH-Mitragynine Flexible Receptor Docking and Binding Pose Alignment.....</i>	<i>5</i>
<i>Flexible Ligand-Rigid Receptor Docking.....</i>	<i>5</i>
<i>Residue Interactions.....</i>	<i>5</i>
C. In-Silico Screening of Mitragynine Analogs.....	6
<i>Analog Design.....</i>	<i>6</i>
<i>SwissADME Pharmacokinetic Filter.....</i>	<i>6</i>
<i>Geometry Optimizations.....</i>	<i>6</i>
<i>Preparation for AutoDock Vina Docking.....</i>	<i>7</i>
<i>Flexible Ligand-Rigid Receptor Docking.....</i>	<i>7</i>
<i>Flexible Ligand-Flexible Receptor Docking.....</i>	<i>7</i>
<i>Residue Interactions.....</i>	<i>8</i>
III. Results and Discussion.....	10
A. Human Mu-Opioid Receptor Homology Modeling.....	10
B. In-Silico Description of Activity in Six Biased Agonists.....	13
C. In-Silico Mitragynine Analog Virtual Screening.....	26

IV. Conclusions.....	54
V. References.....	56

## I. Introduction

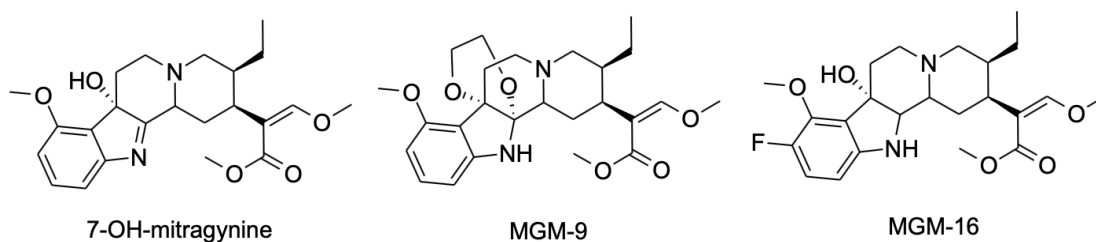
The mu-opioid receptor (MOR) is a G-protein coupled receptor and a major target of opioid pharmaceuticals for the treatment of pain. MOR agonists elicit downstream activation by receptor binding and stimulating a receptor pocket within the active site that is between transmembrane helices (TMH) five and six (2).



**Figure 1: Eight residues of the binding pocket in between TMH 5 (orange) and 6 (yellow) within the mu-opioid receptor active site**

Upon binding, hydrophobic contacts within the binding pocket and hydrogen bonding with the pocket's His299 residue translocate the transmembrane helices, thereby resulting in a conformational change to the intracellular domain (2). Salt-bridge formation by movement of the Lys235 residue has also been associated with mu-opioid receptor activation (3). The conformation change in the intracellular domain results in accessibility for G-protein and  $\beta$ -arrestin binding that activate distinct signaling cascades. The development of MOR agonists that favor or exclusively activate G-protein signaling by MOR binding could lead to pharmaceuticals for pain relief that lack the “negative side effects and high abuse potentials” associated with current opioids (4).

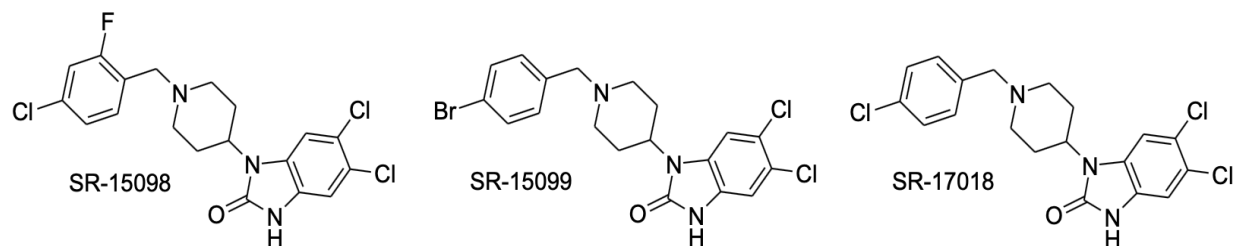
Mitragynine is the dominant alkaloid of the plant, kratom, that is used recreationally in addition to its role in opioid replacement therapy. In 2019, it was discovered that mitragynine undergoes metabolic oxidation by a water nucleophile resulting in imine formation and the addition of a hydroxyl group to the carbon 7 position of the 9-methoxyindole domain (5). This metabolite is considered the active metabolite responsible for analgesic effects by acting as a biased partial agonist at the MOR (5,6). Mitragynine is “atypical” in that its chemical structure is different from other opioids, providing potential for the design of new classes of pain-relieving pharmaceuticals based on its unique chemical structure (6). Recent developments have led to the successful development of closely related mitragynine-analog agonists MGM-9 and MGM-16 (7).



**Figure 2: Active metabolite of mitragynine and two existing analogs agonists**

In 2017, a number of mu-opioid receptor agonists with statistically validated bias for G-protein activation over  $\beta$ -arrestin recruitment for in-vitro assays were identified (Figure 3) (8). Previous studies of supposedly biased agonists, including mitragynine, lacked such verification. For this reason, the activity of SR compounds may help elucidate mitragynine agonist activity and guide mitragynine analog design toward G-protein signaling bias. Although bias cannot be inferred from molecular docking, conservation of the mitragynine scaffold with precise structural changes may allow for the identification of bioisosteres (functional groups with related biological

activity) that can be delivered to the mu-opioid receptor site to expand the number of opioid agonists derived from this class of molecules.



**Figure 3: Three SR agonists with verified G-protein signaling bias**

Developments in protein crystallography, which seek to elucidate the structure of a protein, have led to the discovery of four MOR structures which allows for computational modeling of the receptor and use in docking studies. Existing studies have used molecular docking software to model mitragynine within the active site of the MOR protein's crystal structures and characterized interactions between the ligand and receptor (6). Their findings suggest how mitragynine's unique structure interacts within the active site and can expedite drug design. In this study, the activity of six biased MOR agonists was explored with molecular docking in a homology model of the human mu-opioid receptor to better elucidate their activity and to guide the design of mitragynine analogs. Finally, a virtual screen of pharmacokinetics and molecular docking was performed for a library of 185 compounds designed by bioisostere and aromatic functional group sampling. From this screen, fifteen analogs with aromatic or halogenated modifications to the  $\beta$ -methoxyacrylate domain of mitragynine were identified. The results of this screen represent modifications to the mitragynine scaffold that may deliver more extensive hydrophobic contact and hydrogen bonding to the binding pocket between TMH 5&6.



## II. Methodology

### A. Human Mu-Opioid Receptor Homology Modeling

A human mu-opioid receptor (hMOR) homology model was built with SwissModel using a NCBI BLAST primary amino acid sequence of the human receptor and a crystal structure of the murine receptor (PDB: 5C1M) (9-11). The homology model was prepared for docking with Yasara by adding hydrogen atoms and simulated annealing energy minimization (12).

Ramachandran plots were extracted for the homology model in MOE before and after energy minimization (13). Following minimization, the homology model and the 5C1M template protein structure were aligned in UCSF Chimera and various RMSD aspects were computed (14). The receptor input PDBQT file was prepared in AutoDock ADT by merging non-polar hydrogens, computing Gasteiger charges, and defining grid box size and location (15).

### B. In-Silico Exploration of Activity in Six Mu-Opioid Receptor Biased Agonists

#### *Geometry Optimizations*

HF/6-31+G\* level geometry optimizations in implicit water solvent were accomplished for the six biased agonists in Spartan '16 (16,17). Optimizations were performed in the +1 protonated state for the basic nitrogen atom.

#### *Preparation for AutoDock Vina Docking*

Optimized geometry files were exported from Spartan as PDB files and imported into AutoDock ADT for docking preparation (17,15). Flexible torsions were chosen for each analog and exported as PDBQT files.

### *7-OH-Mitragynine Flexible Receptor Docking and Binding Pose Alignment*

A flexible ligand-flexible receptor calculation of 7-hydroxymitragynine was first performed in AutoDock Vina to identify the correct binding pose for screening binding poses of the other five agonists (18). Binding poses of 7-hydroxymitragynine were superimposed over the 5C1M crystal structure containing the co-crystallized agonist BU72 in PyMOL (19). 7-hydroxymitragynine was aligned according to its previously described binding pose (6). The aligned binding pose and corresponding binding affinity energy values were extracted.

### *Flexible Ligand-Rigid Receptor Docking*

Flexible ligand-rigid receptor docking calculations in AutoDock Vina were performed in the hMOR homology model for the remaining five agonists (18). Docking results were screened by superimposing the five lowest-energy binding poses for each agonist over the alignment of BU72 and 7-hydroxymitragynine. The lowest-distance interactions with residues Asp149 and His299 in the active site were prioritized in alignment given their widely-described roles in opioid binding (1,6). Aligned binding poses and corresponding binding affinity energies were extracted for the five agonists.

### *Residue Interactions*

Ligand interactions with residues of the flexible receptor docking calculation were described to develop the structure-activity relationships of mu-opioid receptor biased agonists. All ligand interactions with receptor site residues within 4.0 Å were measured. Ligand interactions were visually analyzed and correct residue interactions were extracted to describe structure-activity relationships.

## C. In-Silico Screening of Mitragynine Analogs

### *Analog Design*

A compound library of analogs was designed from the lead compound 7-hydroxymitragynine. Analogs were designed by modification of the 9-methoxyindole domain,  $\beta$ -methoxyacrylate substituent, ethyl substituent, translocation of the basic nitrogen atom, and modification of the ring system. Bioisosteres, functional groups with related biological activity, of the phenol, ester, and O-methyl domains were incorporated into analog design (20).

### *SwissADME Pharmacokinetic Filter*

Analogs were submitted to the SwissADME webtool in the non-protonated nitrogen state to predict pharmacokinetic properties (21). Despite the known role of the basic, protonated nitrogen in opioid activity, the webtool was parameterized for neutral compounds. Predicted gastrointestinal (GI) and blood brain barrier (BBB) accessibilities were extracted for each compound.

### *Geometry Optimization*

HF/6-31+G\* level geometry optimization in implicit water solvent was run in Spartan '16 for analogs with predicted GI and BBB accessibility (16,17). Addition of a hydroxyl group before optimization was performed for analogs designed without modification of carbon 7 in the 9-methoxyindole domain. Optimizations were performed in the +1 charge state for the basic nitrogen atom being protonated.

### *Preparation for AutoDock Vina Docking*

Optimized geometry files were exported from Spartan as PDB files and imported to AutoDock ADT for docking preparation (17,15). Torsion angles were chosen for each analog and exported as PDBQT files.

### *Flexible Ligand-Rigid Receptor Docking*

Flexible ligand-rigid receptor docking calculations in AutoDock Vina were performed in the hMOR homology model for analogs retained after the SwissADME screen (18,21). Docking results were screened by superimposing the five lowest-energy binding poses over the alignment of BU72 and 7-hydroxymitragynine. The lowest-distance interactions with residue Asp149 and His299 were prioritized in alignment given its widely-described role in opioid ligand binding (1,6). Analogues with aligned binding poses were then screened against the binding affinity of 7-hydroxymitragynine. Analogues with an equal or lower binding affinity energy to 7-hydroxymitragynine (-8.5 kcal/mol) were retained for flexible ligand-flexible receptor docking calculations. The aligned binding poses and corresponding binding affinity energy was extracted for successfully screened analogues.

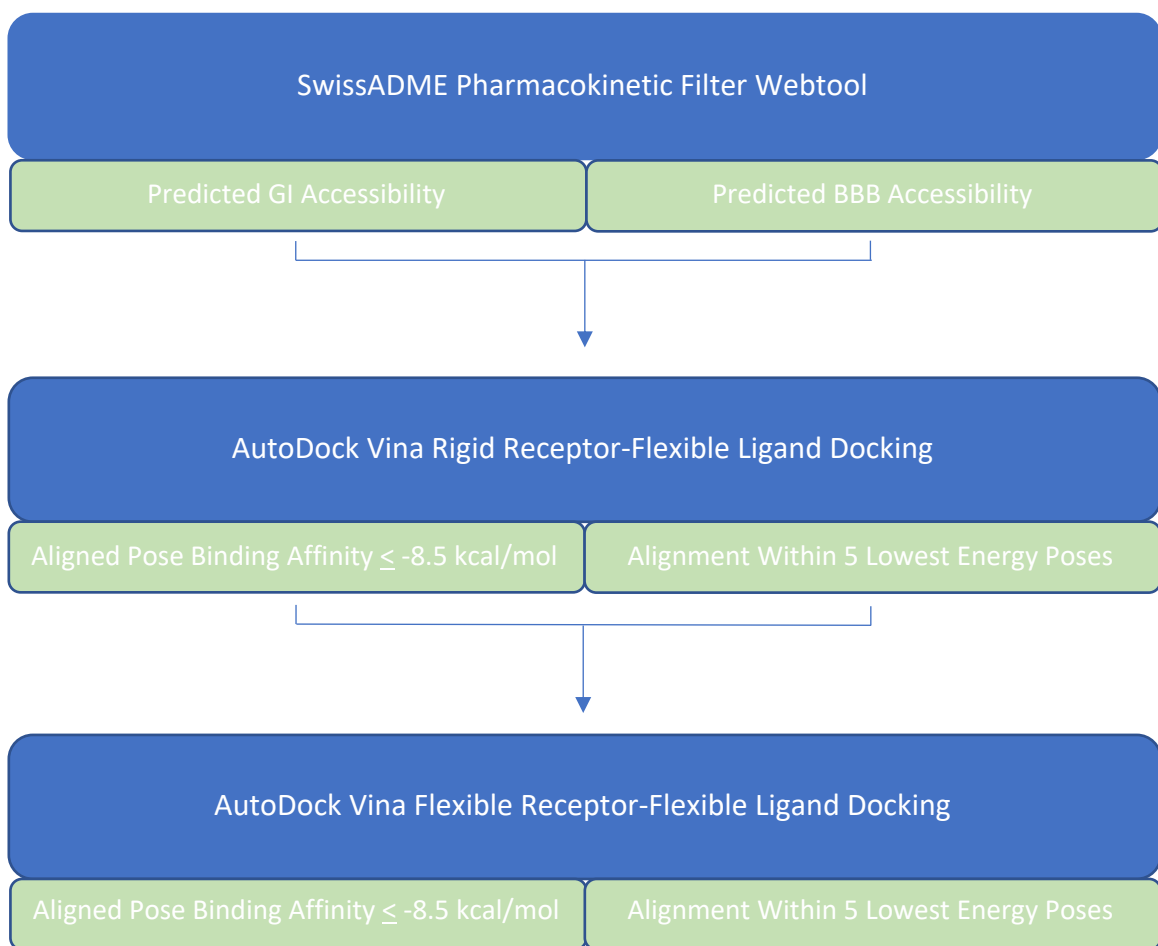
### *Flexible Ligand-Flexible Receptor Docking*

Flexible ligand-flexible receptor docking calculations in AutoDock Vina were performed for retained analogues (18). A flexible receptor of 21 active site residues was constructed in AutoDock ADT before docking calculations (15). Active site residues chosen for the flexible receptor had previously been described in opioid binding of mitragynine and SR agonists from an induced-fit flexible receptor docking study in MOE (2,13). Results were screened by

superimposing the five lowest-energy binding poses over the alignment of BU72 and 7-hydroxymitragynine. The lowest-distance interactions with residue Asp149 and His299 were prioritized in alignment given its widely-described role in opioid ligand binding (1,6). Analogs with aligned binding poses were then screened against the binding affinity of 7-hydroxymitragynine. Analogs with an equal or lower binding affinity energy to 7-hydroxymitragynine (-8.5 kcal/mol) were retained for flexible ligand-flexible receptor docking calculations. The aligned binding poses and corresponding binding affinity energies were extracted for successfully screened analogs.

#### *Residue Interactions*

Ligand interactions with residues of the flexible receptor docking calculation were described to develop the structure-activity relationships of successfully screened mitragynine analogs. All ligand interactions with receptor site residues within 4.0 Å were measured. Ligand-receptor residue interaction distances were analyzed and representative interaction distances extracted to describe structure-activity relationships.



**Figure 4: Representation of the Virtual Screen Utilizing Pharmacokinetic and Molecular Docking Filters**

### III. Results and Discussion

#### A. Human Mu-Opioid Receptor Homology Modeling

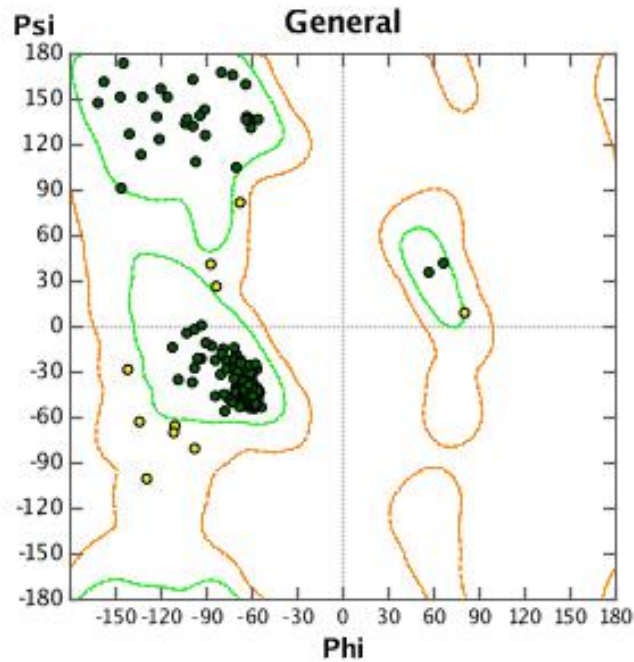


Figure 5: Phi-psi plot of human mu-opioid receptor homology model before energy minimization in Yasara

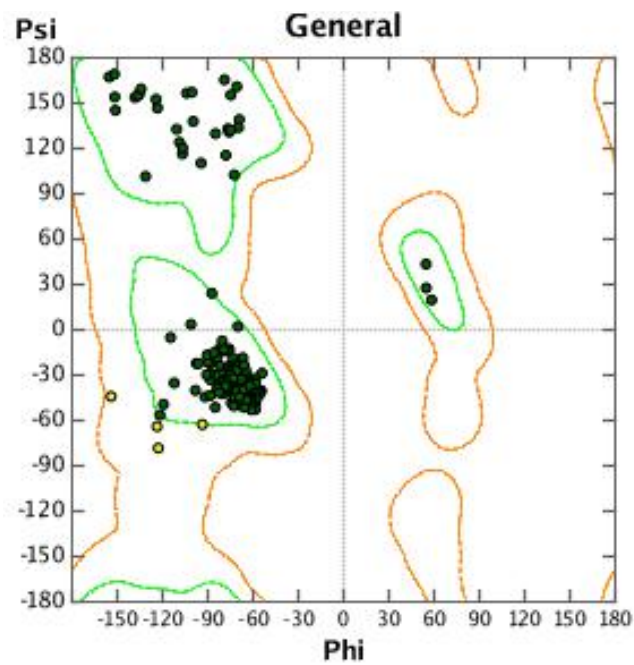
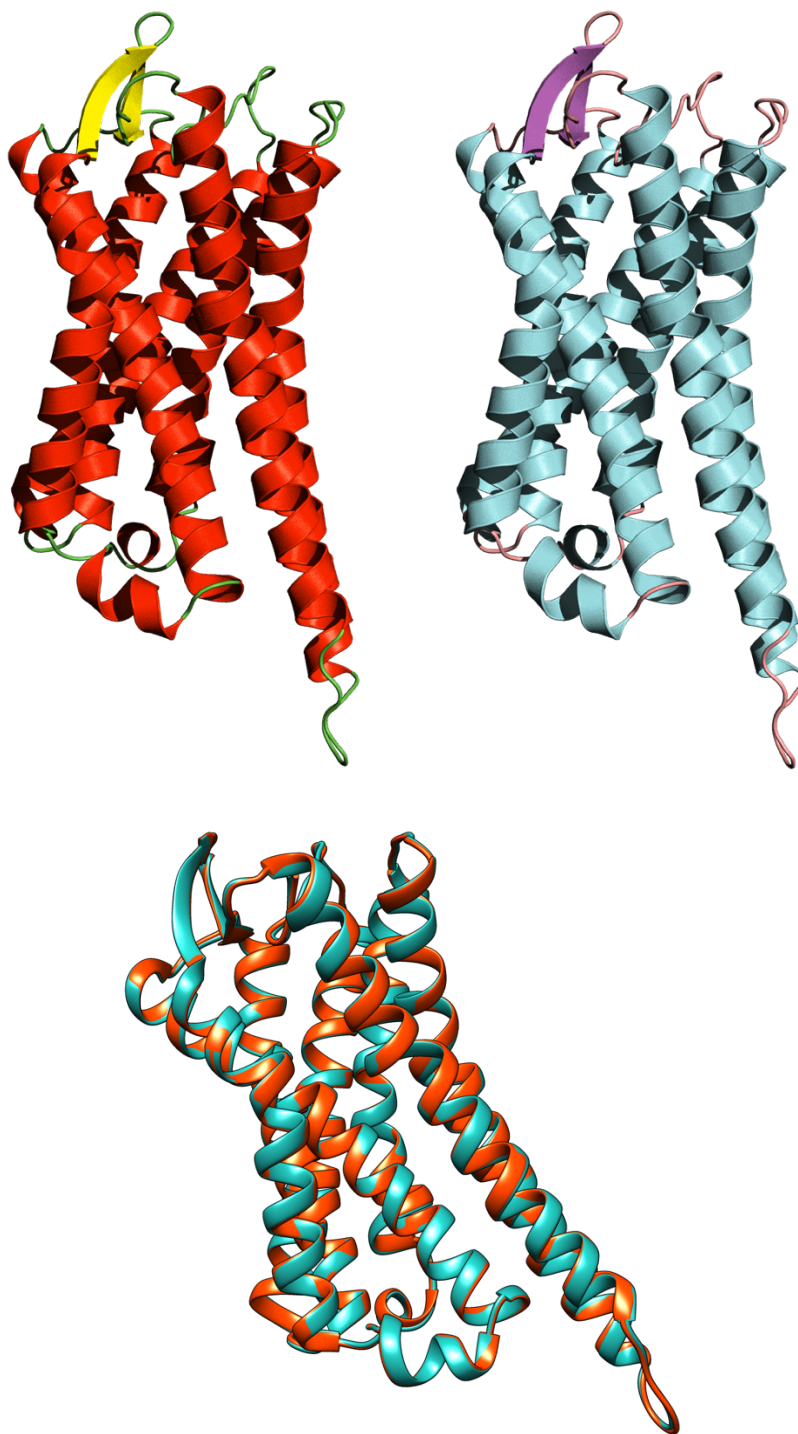


Figure 6: Phi-psi plot of human mu-opioid receptor homology model after energy minimization in Yasara



**Figure 7: Chain A of the murine mu-opioid receptor crystal structure in red (PDB: 5C1M) and energy-minimized SwissModel human mu-opioid receptor homology model in blue with 0.259 Å RMSD alignment between both structures (bottom)**

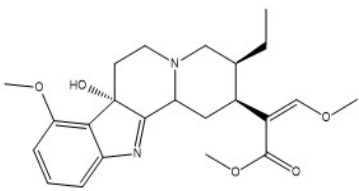
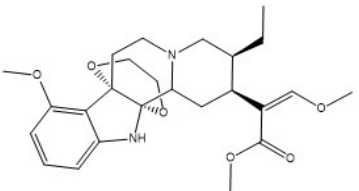
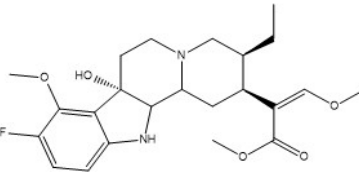
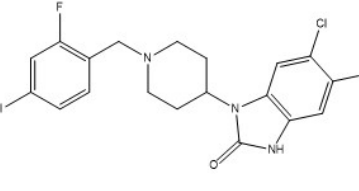
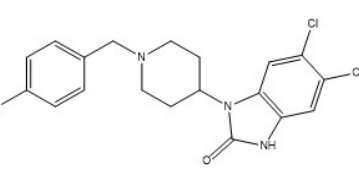
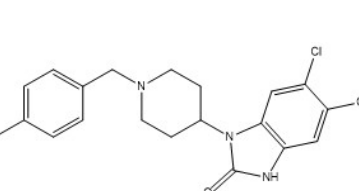


A previous docking study of mitragynine compounds utilized the murine mu-opioid receptor crystal structure (PDB: 5C1M) directly for docking (11). This present study diverged by developing a homology model of the human mu-opioid receptor from the murine receptor template structure for use in docking. The crystallized receptor was captured with a resolution of 2.1 Å and bound with the agonist BU72, thus it represents an activated structure of the mu-opioid receptor (11). The murine receptor crystal structure is composed of two chains, the transmembrane region (Chain A) and the intracellular region (Chain B). The homology model was built solely from transmembrane chain A which contains the entire opioid binding site, sufficient for receptor-ligand docking.

Comparison of the original and minimized models validated the energy minimization. Ramachandran plots generated in MOE for each protein structure revealed that the backbone geometry was improved from ten allowed phi-psi plot points to four (see Figures 5 and 6) (13). Additionally, the homology model was validated against the murine receptor crystal structure. Alignment of the 5C1M crystal structure with the energy-minimized homology model in UCSF Chimera revealed a RMSD = 0.259 Å and confirmed that the homology model was suited for use in ligand docking, as shown in Figure 7 (14). Results of 7-hydroxymitragynine docking (described later) also validated use of the homology model in docking by reproducing the binding pose described by an existing docking study that used the 5C1M crystal structure directly (6).

## B. In-Silico Description of Activity in Six Biased Agonists

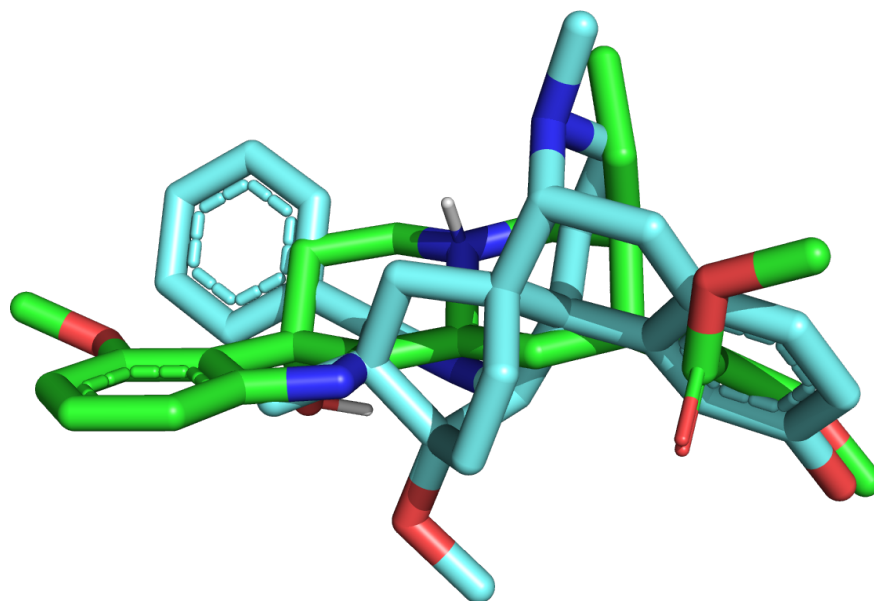
**Table 1: Binding Poses and Binding Affinities of Six Mu-Opioid Receptor Agonists**

Analog		Docking Calculations	
Structure	ID	Output	Flexible Receptor
	7-OH-Mitragynine	Binding Pose	7
		Binding Affinity	-8.5 kcal/mol
	MGM-9	Binding Pose	1
		Binding Affinity	-10.4 kcal/mol
		$\Delta$ 7-OH-Mitragynine	-1.9 kcal/mol
	MGM-16	Binding Pose	5
		Binding Affinity	-9.1 kcal/mol
		$\Delta$ 7-OH-Mitragynine	-0.6 kcal/mol
	SR-15098	Binding Pose	5
		Binding Affinity	-10.4 kcal/mol
		$\Delta$ 7-OH-Mitragynine	-1.9 kcal/mol
	SR-15099	Binding Pose	5
		Binding Affinity	-9.9 kcal/mol
		$\Delta$ 7-OH-Mitragynine	-1.4 kcal/mol
	SR-17018	Binding Pose	2
		Binding Affinity	-11.8 kcal/mol
		$\Delta$ 7-OH-Mitragynine	-3.3 kcal/mol

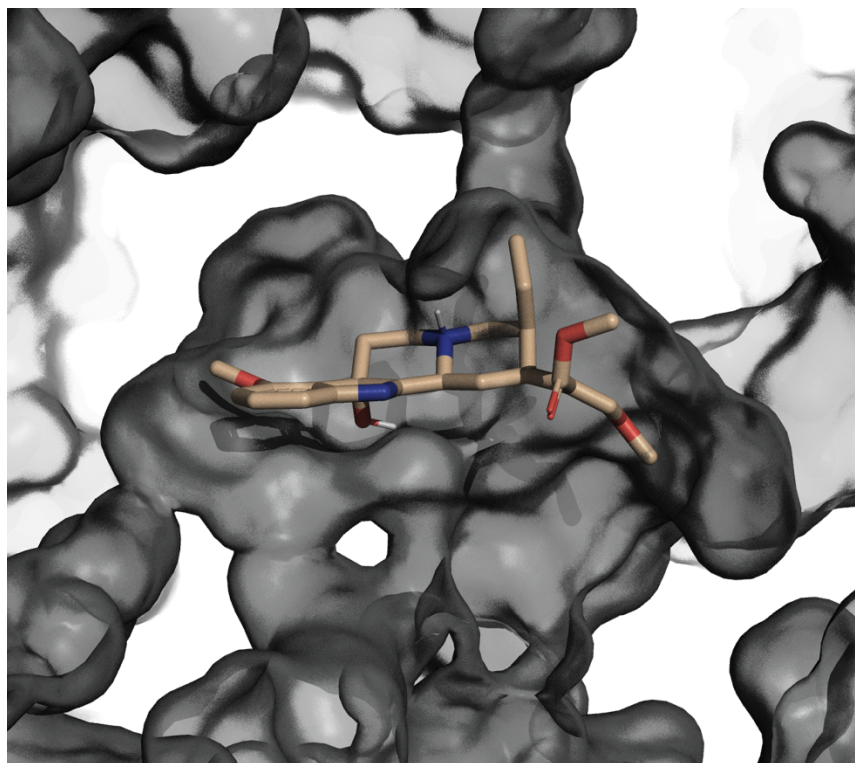
**Table 2: MOR Biased Agonist Active Site Residue Contacts within 4.0 Angstroms**

Active Site Residue	Ligand-Receptor Residue Contacts (Angstroms)					
	7-OH-Mitragynine	MGM9	MGM16	SR-15098	SR-15099	SR-17018
Aspartate 56	4					
Serine 57		3.5	3.1	3.8	3.8	
Glutamine 126	3.5	3.7	3.7	4	3.5	3.5
Tryptophan 135	3.7		3.1, 3.8	3.6		
Valine 145			3.6			
Isoleucine 146		3.8		3.2		
Aspartate 149**	3.2		3.8			
Tyrosine 150**	3.3		3.5	3.7	3.4	3.9
Methionine 153**	3.7, 4.0		3.9	3.7, 3.8	3.8, 3.9	
Cysteine 219			3.9	4		
Lysine 235	3.8				3.8	
Valine 238	3.8	3.6	3.8, 4.0	3.7	3.7	3.7, 3.8
Tryptophan 295**	3.8	3.7	3.7		3.6	3.8
Isoleucine 298	3.7	3.7, 3.8	3.6	2.8	3.1, 3.4	2.5
Histidine 299**	3.9	3.7		3.3	3.4, 3.9	2.9, 3.9
Valine 302		3.6, 3.6	3.9	3.5	3.8, 3.9	3.8
Lysine 305						
Tryptophan 320	3.6	3.6, 3.7				3.7
Histidine 321*	4				3.8	3.8
Isoleucine 324	3.7	2.9	3.8		3.7, 3.9	3.8, 4.0
Tyrosine 328*	3.3, 3.6	3.3, 3.7	1.9	4	3.8	3.9

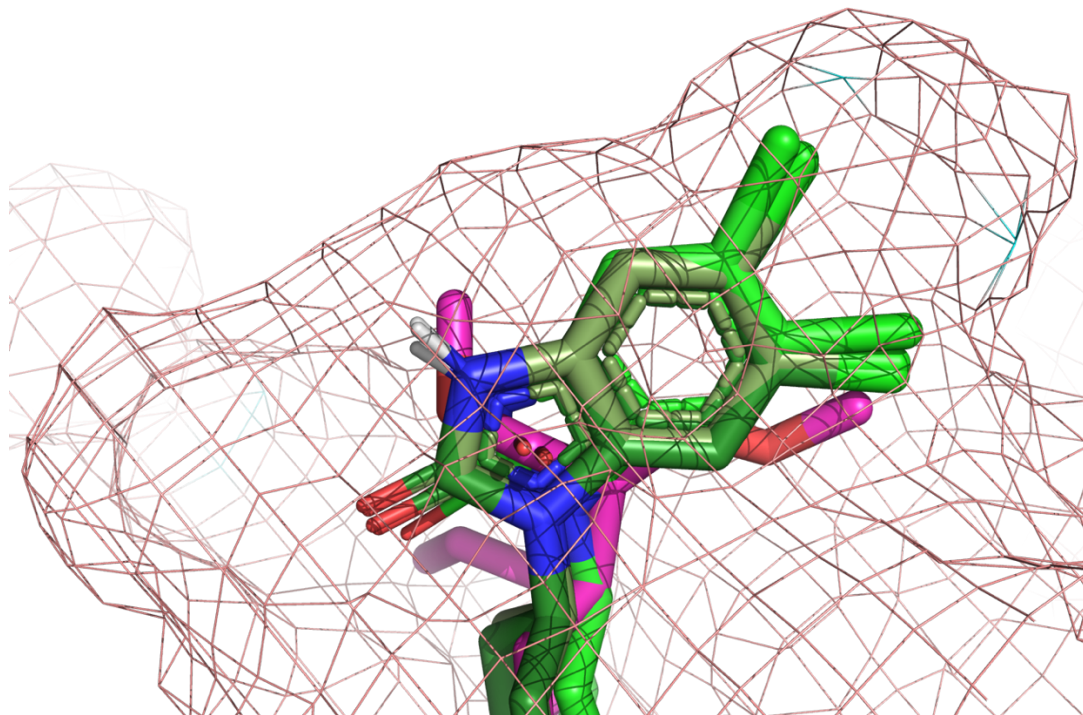
*Note: Two values designate two distinct interactions of the ligand and active site residue*



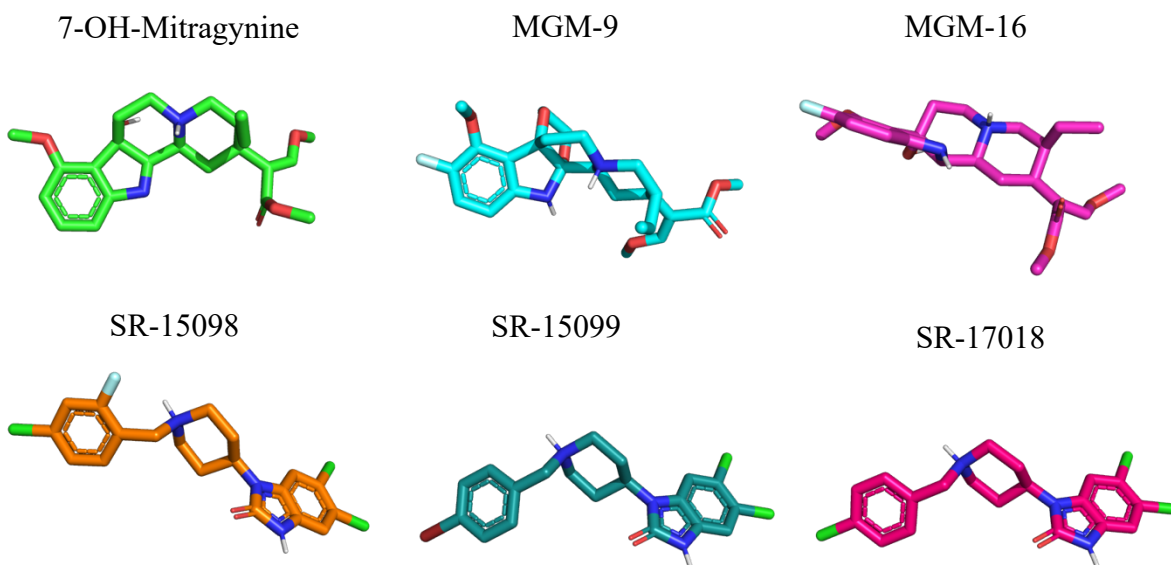
**Figure 8: Alignment of 7-OH-mitragynine binding pose (green) and BU72 agonist (blue) co-crystallized in 5C1M murine mu-opioid receptor crystal structure previously described (6)**



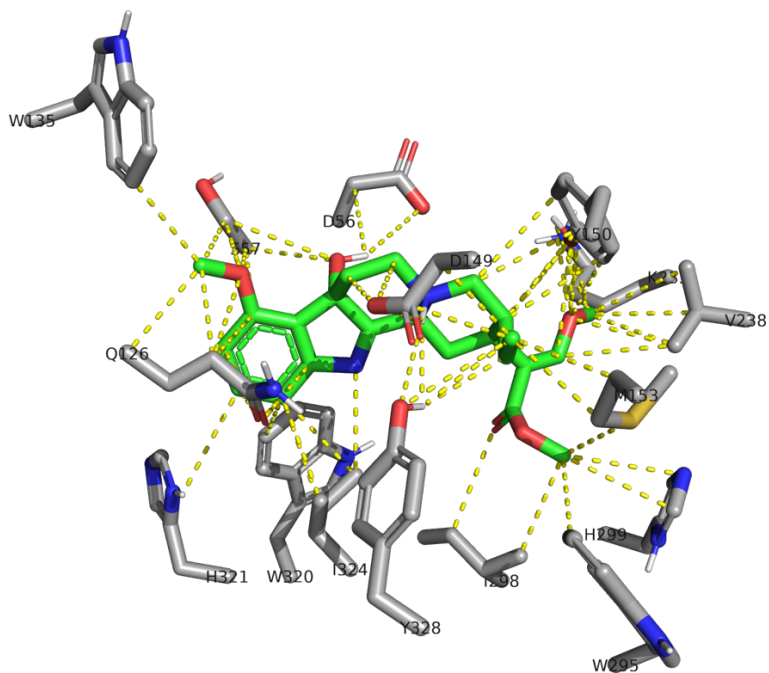
**Figure 9: Binding pose of 7-OH-Mitragynine in active site styled by receptor surface  
(receptor in upside-down orientation)**



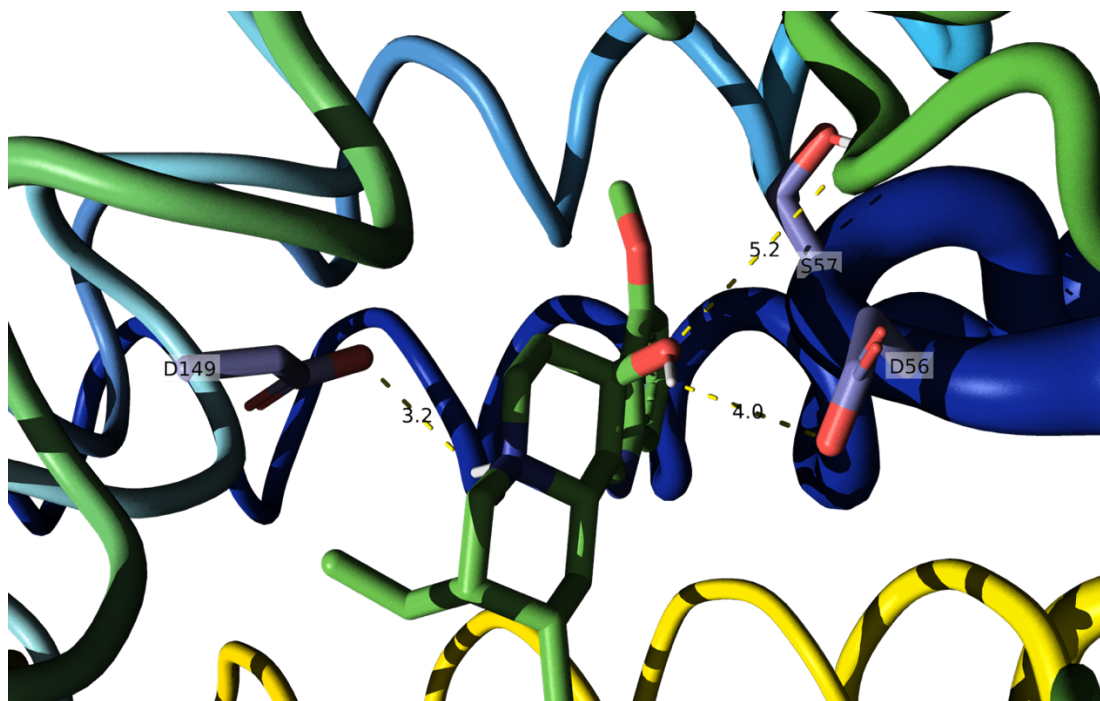
**Figure 10: Binding pocket between transmembrane helices 5&6 of human mu-opioid receptor overlapped 7-OH-Mitragynine and SR biased agonists**



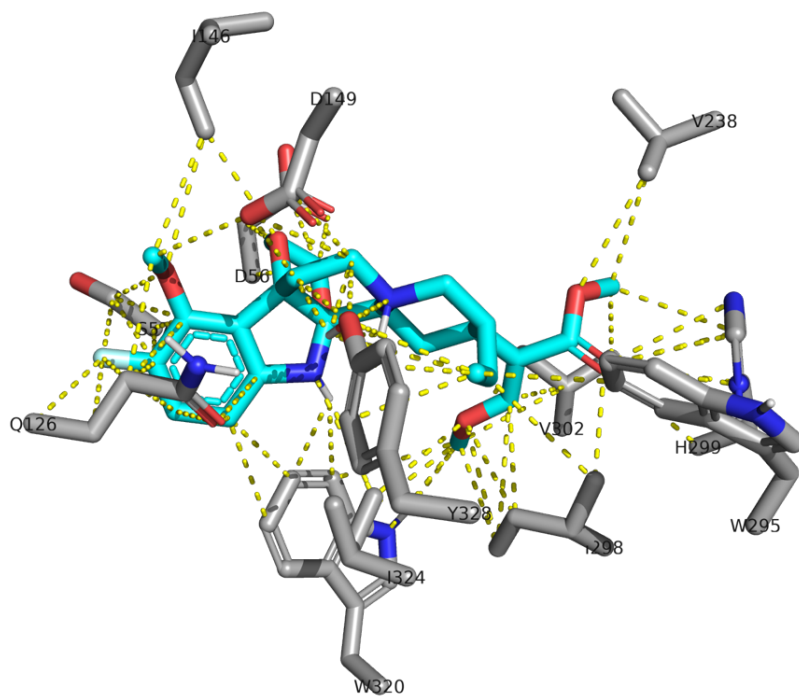
**Figure 11: Binding poses of six mu-opioid receptor biased agonists in grid view**



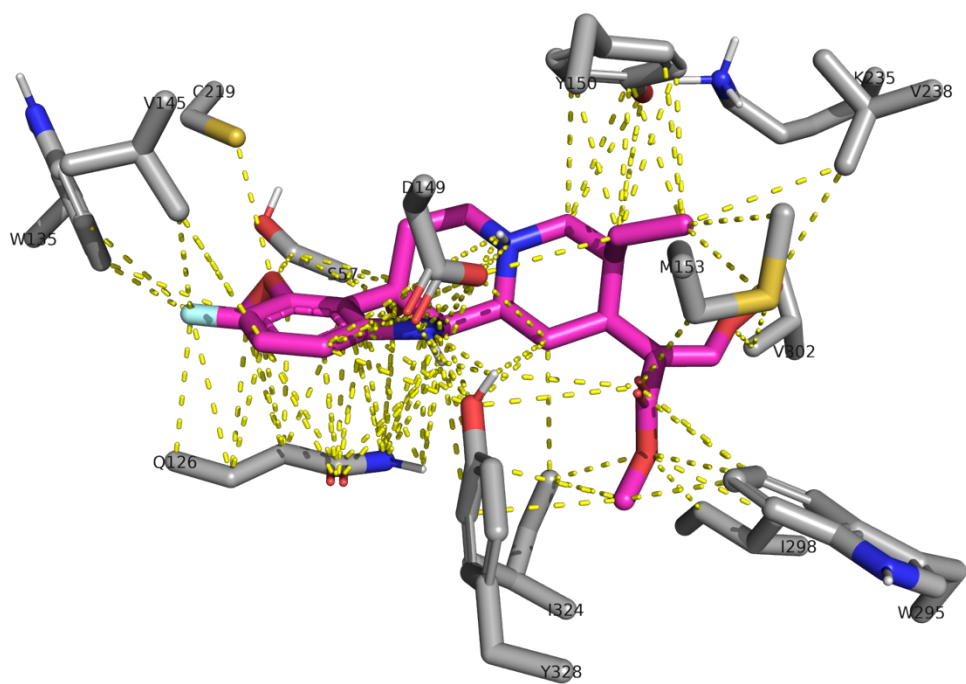
**Figure 12: 7-OH-Mitragynine active site residue contacts within 4.0 Å**



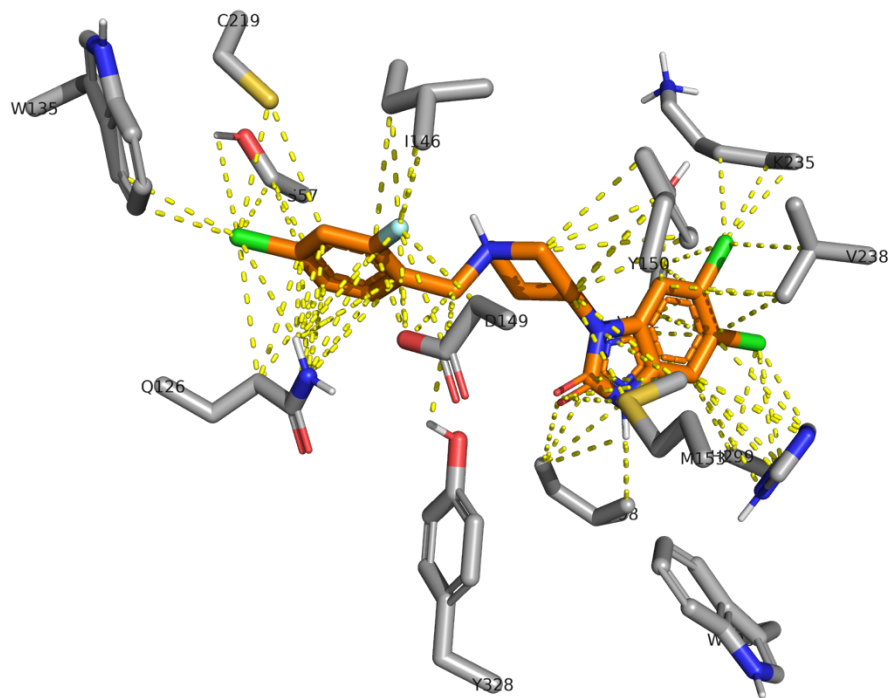
**Figure 13: Hydrogen bonding network between 7-OH-Mitragynine and residues Aspartate 56, Serine 57, and Aspartate 149 enabled by oxidation at the Carbon-7 position. Protein model is rendered with beta-factor to convey flexibility of loop overlaying active site**



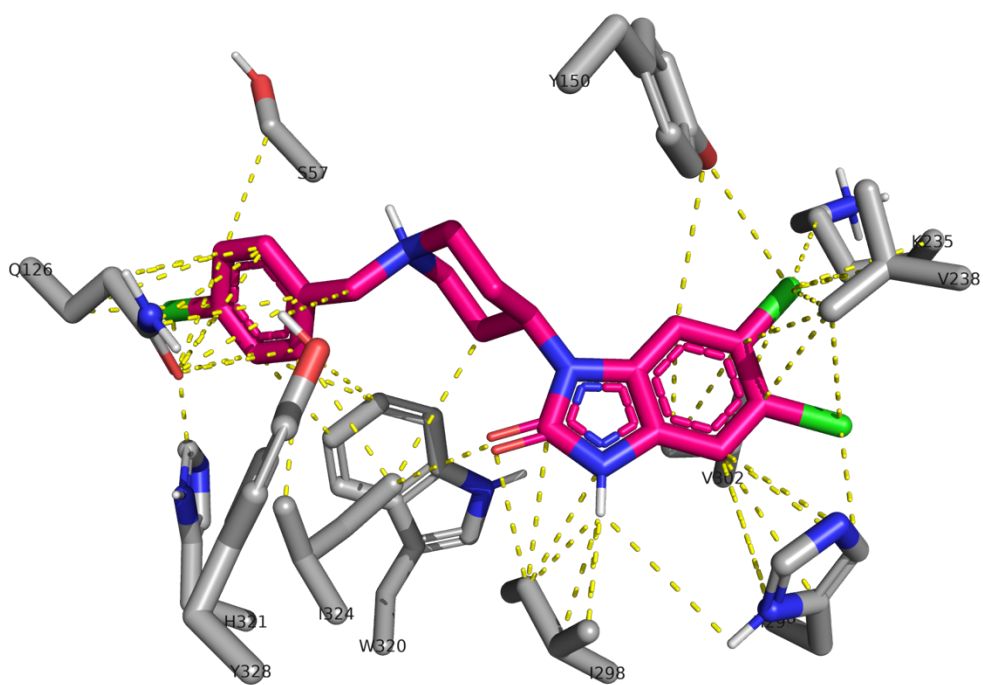
**Figure 14: MGM-9 active site residue contacts within 4.0 Å**



**Figure 15: MGM-16 active site residue contacts within 4.0 Å**

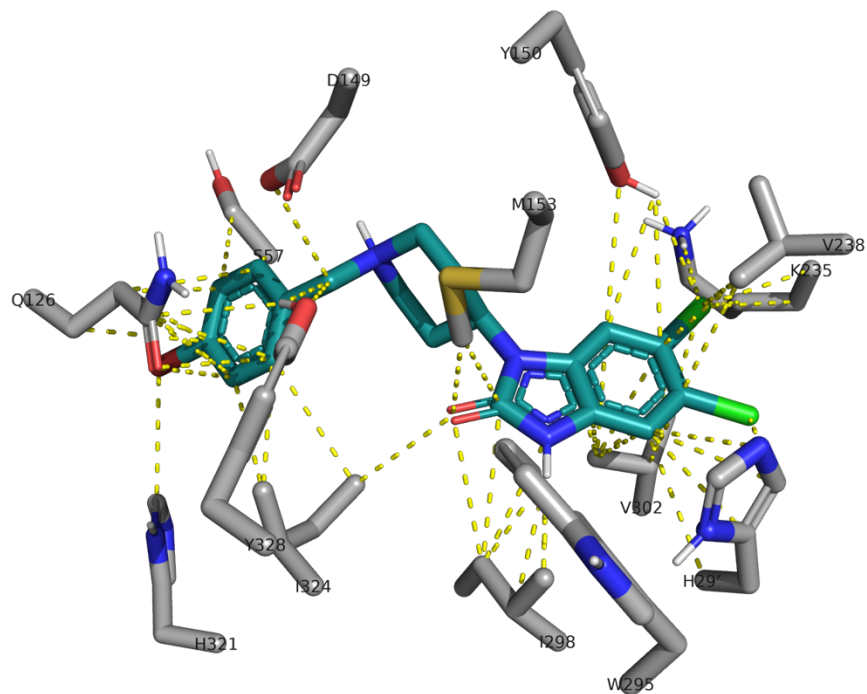


**Figure 16: SR-15098 active site residue contacts within 4.0 Å**

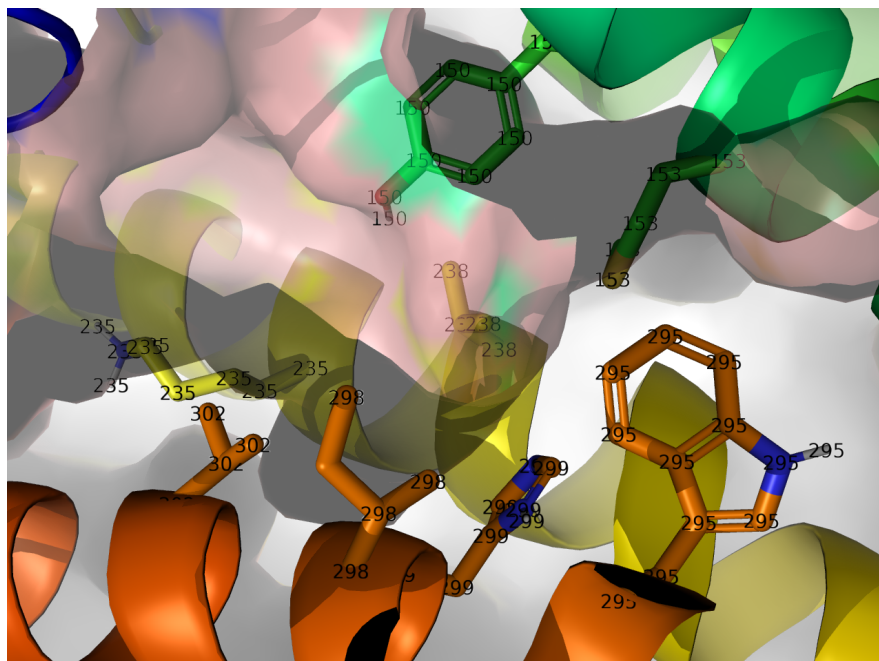


**Figure 17: SR-15099 active site residue contacts within 4.0 Å**

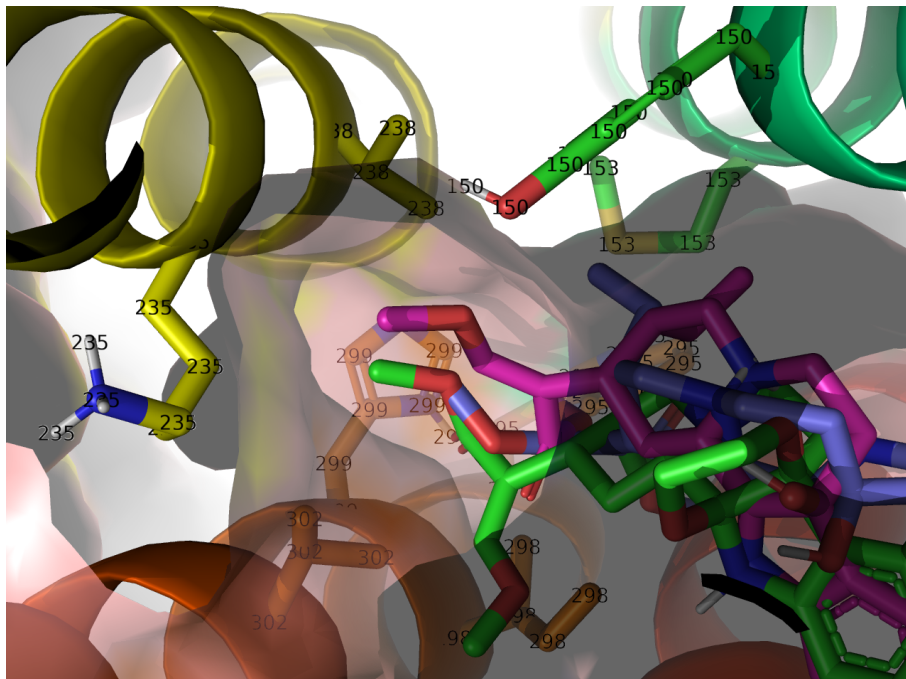




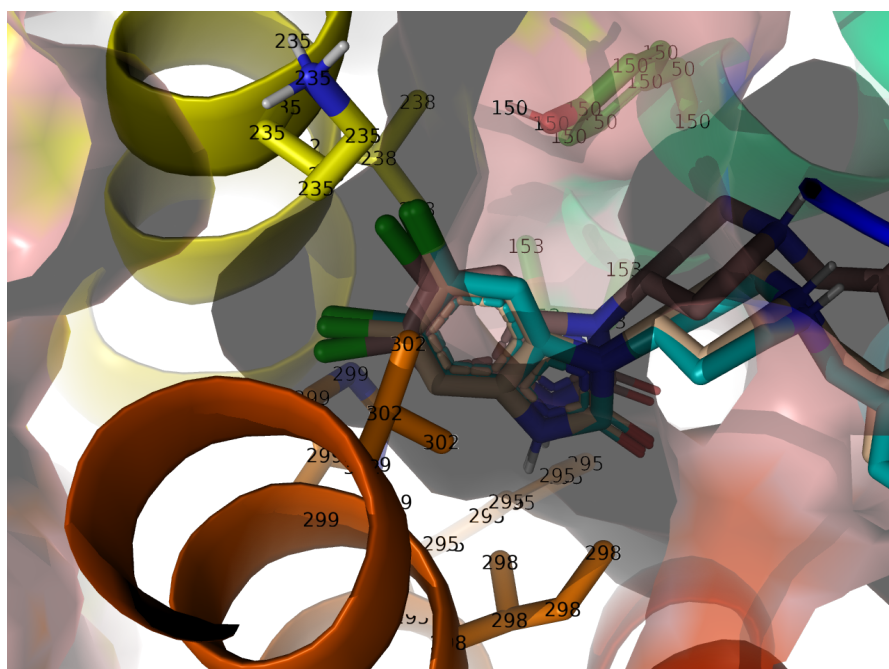
**Figure 18: SR-17018 active site residue contacts within 4.0 Å**



**Figure 19: Eight residues of the TMHs 5 and 6 human mu-opioid receptor binding pocket with opaque surface rendering to visualize the intrahelical binding pocket**



**Figure 20: 7-OH-mitragynine and MGM-16 direct enol ether while MGM-9 directs methyl ester to TMH5&6 binding pocket**



**Figure 21: SR-15098, SR-15099, and SR-17018 direct o-dichlorobenzene of 5,6-dichloro-2H-benzo[d]imidazol-2-one functional group to TMH5&6 binding pocket**

Flexible docking results revealed improved docking scores and lower binding affinities for MGM-9, MGM-16, SR-15098, SR-15099, and SR-17018 compared to the lead compound 7-OH-mitragynine (Table 1). The binding pose score (Pose 7 of 9) of 7-OH-mitragynine was unexpected given that this pose was the highest scored, lowest energy configuration in a previous docking study (6). Replication of the binding pose from this study was validated according to the described alignment with the co-crystallized agonist BU72 (Figure 8).

Alignment of all six biased agonists which represent two classes of opioid agonists revealed the overlap of similar molecular features within the binding site. The position of the basic nitrogen atom with residue Asp149 was expected. In addition, alignment suggests that the substituted indole and substituted benzene of MGM/mitragynine and SR compounds, respectively, have similar binding poses within the receptor site. The most significant finding from alignment was the overlap of the  $\beta$ -methoxyacrylate domain of MGM/mitragynine compounds and the 5,6-dichloro-2H-benzo[d]imidazol-2-one functional group of the SR compounds (see Figure 10). This finding was surprising given the size difference of the two substituents. However, both the  $\beta$ -methoxyacrylate and 5,6-dichloro-2H-benzo[d]imidazol-2-one groups contain electronegative atoms and conjugation, which may inform their overlap within the active site.

Residue contacts were analyzed from results of flexible receptor-flexible ligand docking in a 21-residue active site (Table 2). All residue contacts within 4.0 Å were generated through PyMOL features and subsequently analyzed to better describe residue-ligand interactions (19). In the three MGM/mitragynine agonists, the substituted indole domain binds a pocket containing several aromatic residues: Trp135, His321, and Trp320. This pocket also contains residues Leu324 and Gln126. Gln126 appear to associate in parallel with the benzene ring of the indole

domain (Figures 12,14,15). Several of these residues were previously described; however, the residue Gln126 has not been previously described from mitragynine docking and may be essential to indole domain binding of this pocket (6).

The existing structure-activity relationship of 7-OH-mitragynine suggests that the 7-hydroxyl group merely alters the molecule's conformation compared to mitragynine and proposes that conformational change is the basis for the drastically improved efficacy of 7-OH-mitragynine (5,6). This study discovered that the 7-hydroxyl group was oriented towards the flexible loop overlying the active site. Of interest was the 4.0 Å contact of the 7-hydroxyl group with Asp 56 of this flexible loop notably unobserved for the other five agonists. This finding suggests that the greater affinity of 7-OH-mitragynine may be driven by hydrogen bonding between the ligand the flexible loop over the active site, which may stabilize the ligand-receptor complex. The additional ring of MGM-9 containing two oxygen atoms may also represent a similar ligand-receptor interaction for the mitragynine scaffold (Fig. 14). Figure 13 demonstrates essential hydrogen bonding of the basic N with Asp 149 as well as hydrogen bonding observed between the hydroxyl and Asp 56. The hydrogen bonding distance was also measured between the hydroxyl group and Ser 57, as four of the other five agonists had contact with this adjacent residue within 4.0 Å but not Asp 56. Figure 13 was rendered by beta-factor (temperature factor) which confirmed the greater flexibility of the flexible loop over the binding site. Despite the discovery of hydrogen bonding between five biased agonists and the active site loop, the greater flexibility of this loop reduces the confidence of its location and its orientation may be a product of crystallization rather than an indicator of a role in ligand binding. Future molecular dynamics studies are required to demonstrate any role of the flexible loop in ligand binding.

The ethyl substituent of the MGM/mitragynine agonists has been described as essential to activity and is considered analogous to the N-methyl substituents of many other opioid agonists in which hydrophobic contacts stabilize the basic nitrogen – Asp149 residue interaction (6). Analysis of the 7-OH-mitragynine binding pose reveals that the ethyl substituent is directed into a deep, narrow binding pocket containing residues Met153, Tyr150, and Tyr328 (Figure 1 and Figure 9). (6). Interestingly, the interaction of the ethyl substituent with residue Trp293 has been described for 7-OH-mitragynine but was only observed for MGM-9.

This study presents the discovery of additional residue contacts between 7-OH-mitragynine that have not been previously described. Residue contacts were defined as ligand-residue contacts within 4.0 Å and generated by the contact feature in PyMOL (19). Interactions with eight additional residues were observed. The 9-methoxyindole domain made four additional contacts with Gln126, Trp135, Trp320, and Ile324 representing hydrophobic and aromatic contacts. Trp135 makes a hydrophobic contact with the O-methyl substituent, while the other three residues make contact with the benzene ring of the indole. Three additional contacts were also discovered for the  $\beta$ -methoxyacrylate domain at transmembrane helices 5&6. Namely, two hydrophobic contacts were observed between the enol ether O-methyl and ester O-methyl with Val238 and Ile298, respectively. Finally, contact between the enol ether O-methyl with the alkyl chain of Lys235 was observed. This residue has previously been described in the formation of a salt bridge upon opioid binding (3).

The binding poses of the three MGM/mitragynine agonists revealed similar but distinct conformations. In MGM-9, the dashed  $-O-CH_2-CH_2-O-$  ring of the indole domain restrained conformational flexibility while the lack of an imine group in MGM-16 increased flexibility. Surprisingly, in MGM-9 the basic nitrogen atom was orientated away from Asp 149 residue

despite an otherwise conserved pose with the other two agonists. In addition, while common positioning of the  $\beta$ -methoxyacrylate group was observed, MGM-9 was bound with the methyl ester oriented toward the binding pocket of TMH5 and TMH6, and unlike the enol ether of 7-OH-mitragynine and MGM-16 (see Figure 20).

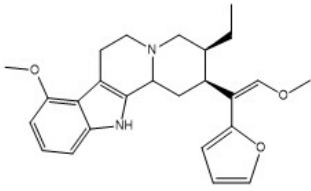
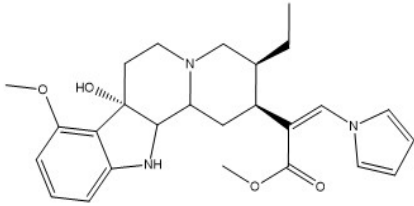
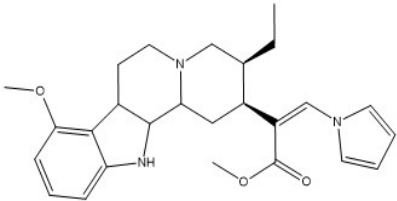
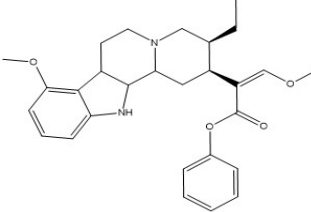
The most surprising finding from docking of the three SR agonist was that their basic nitrogen atoms were oriented adjacent to Asp 149 with a small distance between the residue and atom (see Figures 11, 16-18). This differed from the expected orientation of the basic nitrogen directly towards Asp 149 for this essential residue interaction. As previously mentioned, the alignment of their 5,6-dichloro-2H-benzo[d]imidazol-2-one group with the  $\beta$ -methoxyacrylate group of the MGM/mitragynine agonists was also unexpected largely because of their differences in size. Interaction with the binding pocket between TMH5 and TMH6 was enabled by the 5,6-dichloro-2H-benzo[d]imidazol-2-one functional group. All SR agonists had closer contact with the His299 residue that may reflect greater association by aromatic  $\pi$ -stacking, an interaction the mitragynine scaffold does not deliver to this binding pocket. Additionally, the 5,6-dichloro-2H-benzo[d]imidazol-2-one group may enable greater hydrogen bonding with its carbonyl, two nitrogen atoms, and two chlorine atoms compared to the three oxygen atoms in the ester and enol ether of the  $\beta$ -methoxyacrylate group. However, hydrophobic residue contacts were conserved between SR and MGM/mitragynine agonists. To specify, Val238 and Ile298 contacts were shared. SR agonists showed contact between the halogen groups of the substituted benzene group and Ser57, which may reflect analogous activity of the 7-hydroxyl group of the MGM/mitragynine agonists.

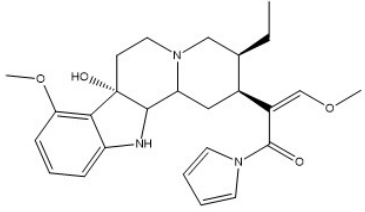
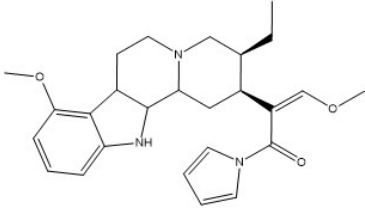
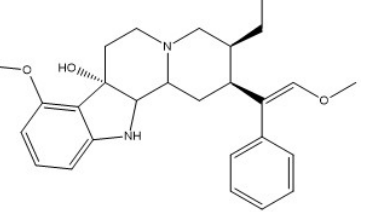
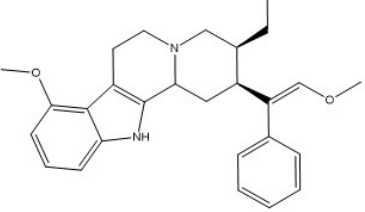
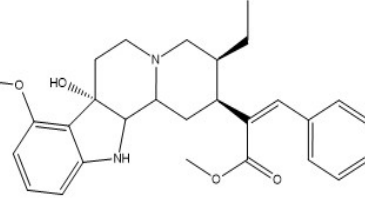
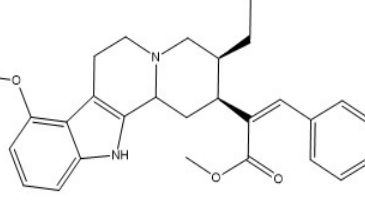
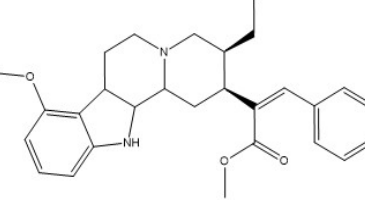
After alignment of the 5,6-dichloro-2H-benzo[d]imidazol-2-one and  $\beta$ -methoxyacrylate groups, further investigation of the binding pocket between TMH5 and TMH6 was warranted.

Overlap demonstrated that the o-dichlorobenzene moiety made deeper contact with the binding pocket than the enol ether of MGM/mitragynine agonists (see Figure 10). Planarity of the 5,6-dichloro-2H-benzo[d]imidazol-2-one functional group may enable greater contact with the binding pocket than the enol ether bent O-methyl. Further description of this binding pocket is continued in discussion of the successfully screened mitragynine analogs.

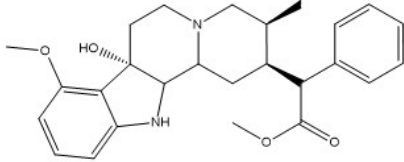
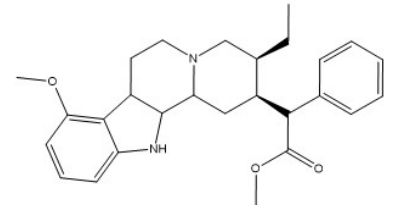
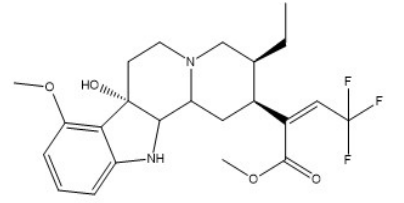
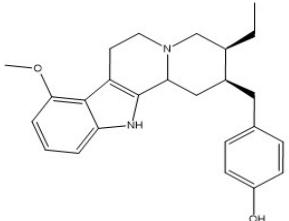
### C. In-Silico Mitragynine Analog Virtual Screening

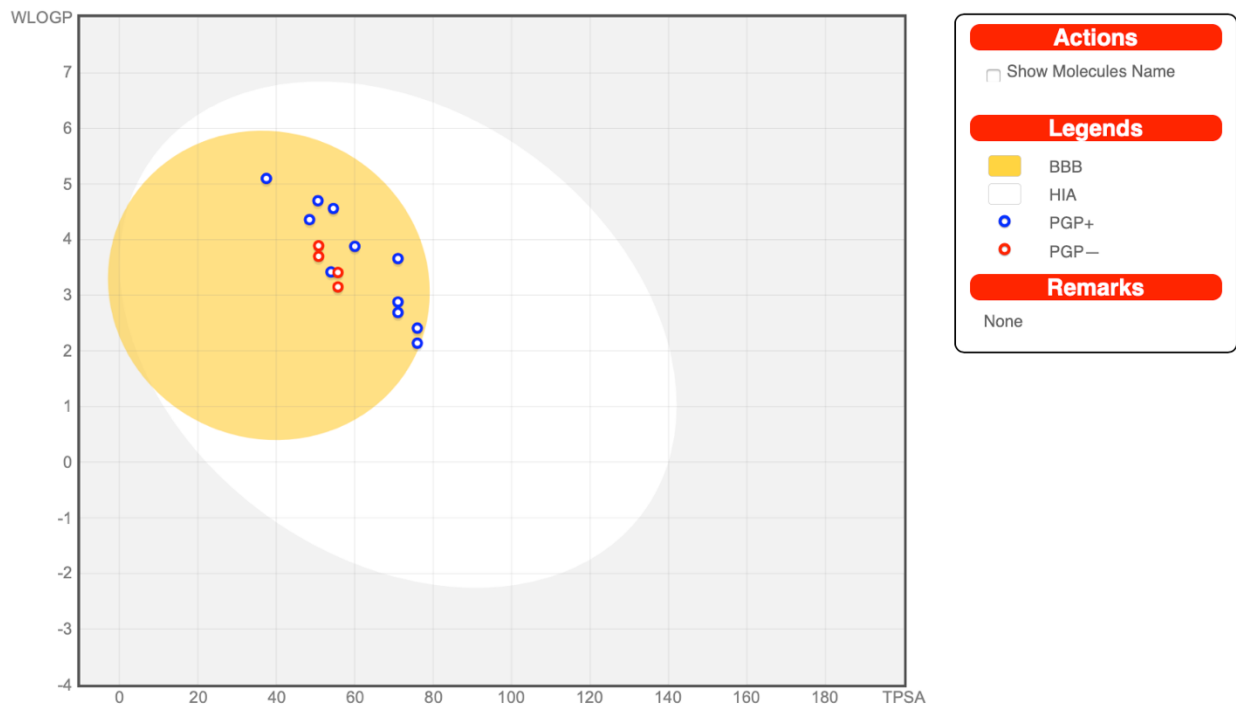
**Table 3: Binding Poses and Binding Affinities of Fifteen Mitragynine Agonists**

Analog		Docking Calculations		
Structure	ID	Output	Rigid Receptor	Flexible Receptor
	R1-25	Binding Pose	4	3
		Binding Affinity	-8.5	-9.7
		$\Delta$ 7-OH-Mitragynine	0	-1.2
	2-7A	Binding Pose	1	1
		Binding Affinity	-9	-10.5
		$\Delta$ 7-OH-Mitragynine	-0.5	-2
	2-7C	Binding Pose	3	2
		Binding Affinity	-8.8	-9.7
		$\Delta$ 7-OH-Mitragynine	-0.3	-1.2
	2-8C	Binding Pose	3	4
		Binding Affinity	-9.6	-11.5
		$\Delta$ 7-OH-Mitragynine	-1.1	-3

	2-9A	Binding Pose	2	1
		Binding Affinity	-9.4	-10.8
		$\Delta 7$ -OH-Mitragynine	-0.9	-2.3
	2-9C	Binding Pose	5	2
		Binding Affinity	-9.2	-9.6
		$\Delta 7$ -OH-Mitragynine	-0.7	-1.1
	2-15A	Binding Pose	1	3
		Binding Affinity	-9.9	-10.8
		$\Delta 7$ -OH-Mitragynine	-1.4	-2.3
	2-15B	Binding Pose	4	3
		Binding Affinity	-8.8	-10.7
		$\Delta 7$ -OH-Mitragynine	-0.3	-2.2
	2-18A	Binding Pose	1	2
		Binding Affinity	-10	-11.3
		$\Delta 7$ -OH-Mitragynine	-1.5	-2.8
	2-18B	Binding Pose	1	1
		Binding Affinity	-8.9	-10.9
		$\Delta 7$ -OH-Mitragynine	-0.4	-2.4
	2-18C	Binding Pose	2	2
		Binding Affinity	-9.7	-10.9
		$\Delta 7$ -OH-Mitragynine	-1.2	-2.4

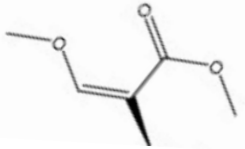

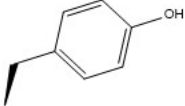
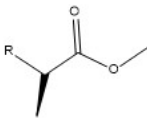
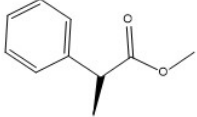
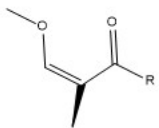
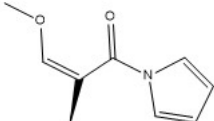
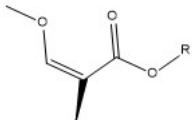
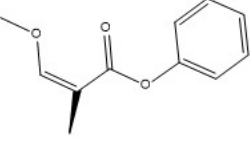
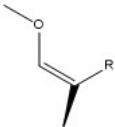
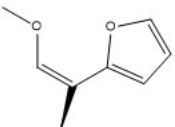
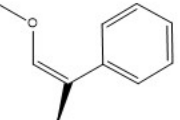
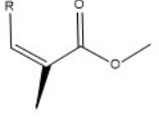
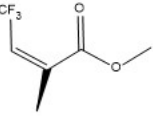
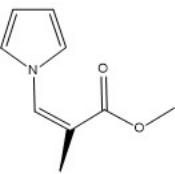
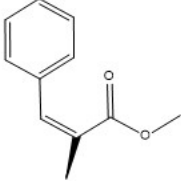


	2-19A	Binding Pose	2	4
		Binding Affinity	-9.3	-10.9
		$\Delta 7$ -OH-Mitragynine	-0.8	-2.4
	2-19C	Binding Pose	2	2
		Binding Affinity	-9.1	-11.2
		$\Delta 7$ -OH-Mitragynine	-0.6	-2.7
	2-21A	Binding Pose	4	1
		Binding Affinity	-8.7	-10.4
		$\Delta 7$ -OH-Mitragynine	-0.2	-1.9
	2-39C	Binding Pose	3	1
		Binding Affinity	-8.8	-10.7
		$\Delta 7$ -OH-Mitragynine	-0.3	-2.2



**Figure 22: Hard-Boiled Egg Diagram for the Fifteen Successfully Screened Mitragynine Analogs Indicating Predicted Gastrointestinal (HIA) and Blood-Brain Barrier (BBB) Accessibilities**

**Table 4: Classes of  $\beta$ -methoxyacrylate substitutions in successfully screened analogs**

 $\beta$ -methoxyacrylate	
	 2E-39
	 2-19A&C
	 2-9A&C
	 2C-8
	 R1-25  2-15A&B
	 2-21A  2-7A&C  2-18A-C

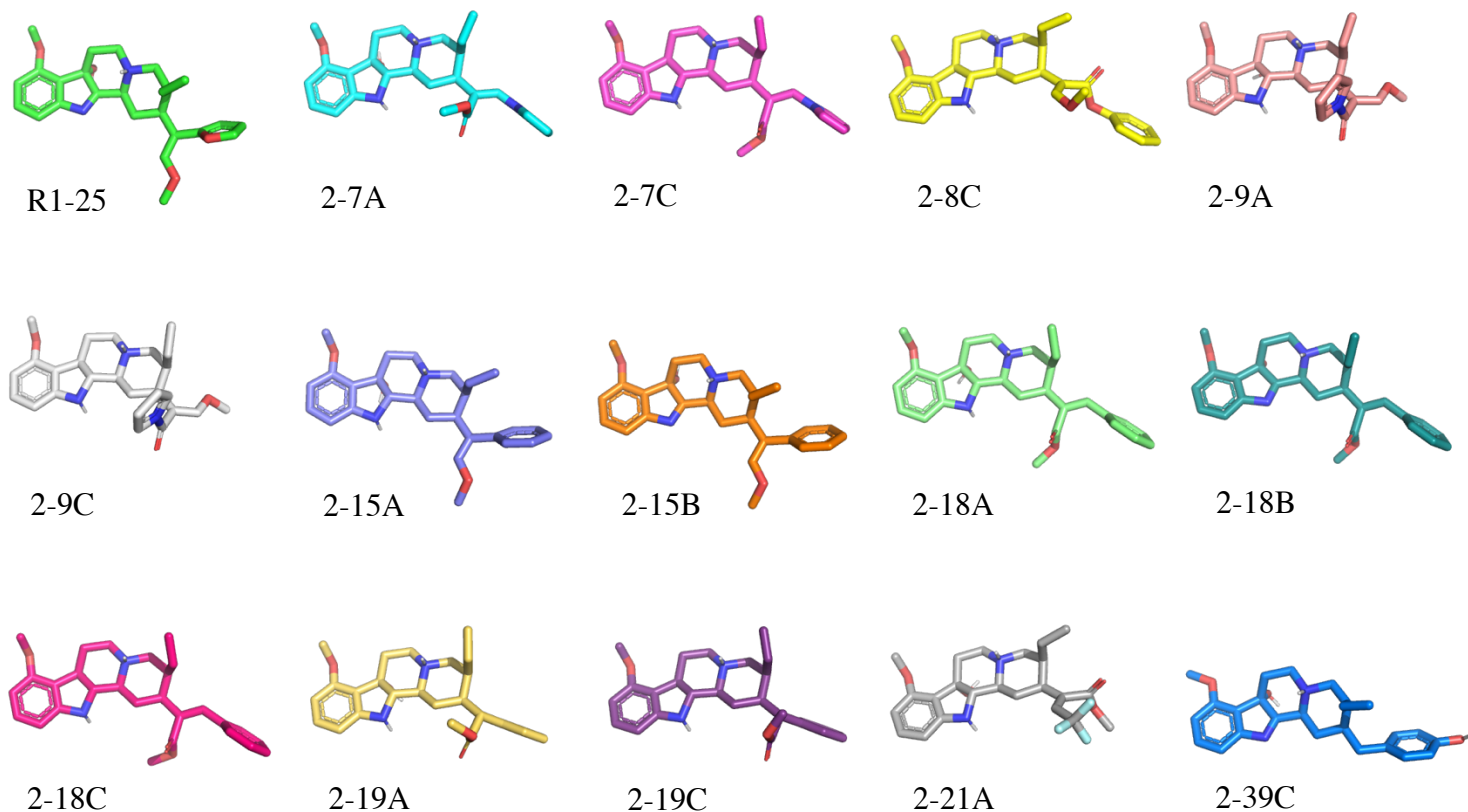
*(Note: Orientation does not indicate binding pose)*

**Table 5: Mitragynine Phenyl/Phenol Substituted Analog – Active Site Residue Contacts  
within 4.0 Angstroms**

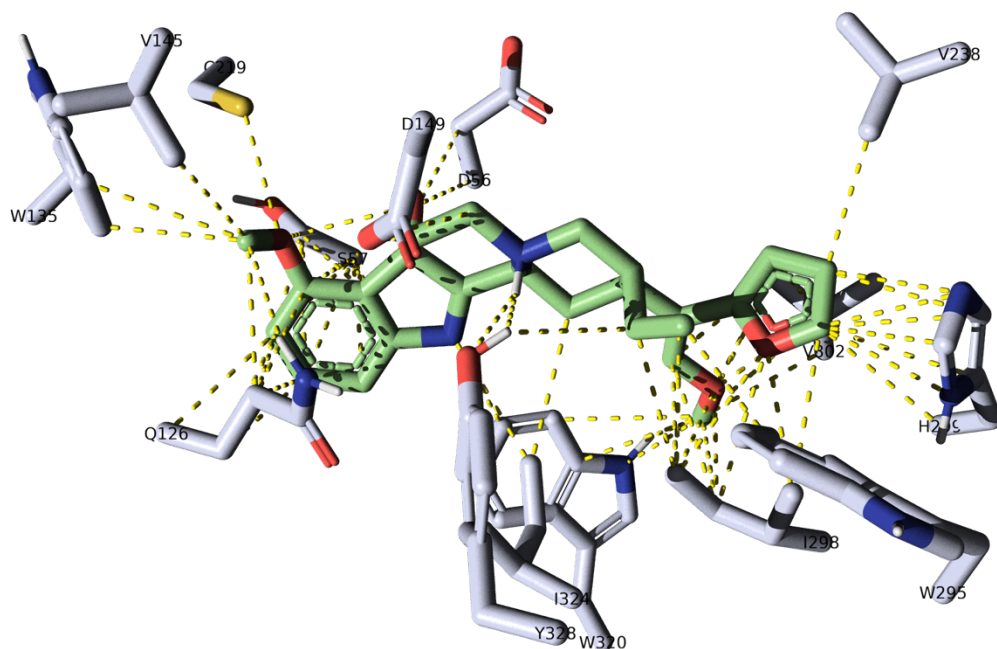
Receptor Residues	Indole Alkaloid Analogs									
	7-OH-M	2-8C	2-15A	2-15B	2-18A	2-18B	2-18C	2-19A	2-19C	2-39E
Aspartate 56	4.0		3.8							
Serine 57		3.5	3.6	1.9,3.1	3.8	3.6,3.8	3.8	3.5	3.5	3.6
Glutamine 126	3.5	4.0	3.8	3.9	3.7	3.7	3.8	3.8,3.9	3.8	3.7
Tryptophan 135	3.7	3.2	3.8	3.7	3.5	3.4	3.5	3.6		3.5
Valine 145					3.6	3.7	3.5	3.9	4.5	
Isoleucine 146		3.7		2.7,3.8	3.6	3.8,4.0	3.6			
Aspartate 149	3.2	2.3	4.0	4.3	3.2	3.5	3.2	3.1	3.4	4.5
Tyrosine 150	3.3	2.9,3.6	3.7		3.8	3.6,3.8	3.7,3.7	3.7,3.8	3.6,3.8	3.8
Methionine 153	3.7,4.0	3.6,3.9	4.0			3.9		4.0	3.9	
Cysteine 219					3.9	3.1,3.6		3.8		
Lysine 235	3.8	2.8			3.7	3.9	3.8	4.0	3.6	
Valine 238	3.8	3.7		3.7	3.9	3.9	3.9	3.6	3.5	3.8
Tryptophan 295	3.8	3.6							3.8	3.7
Isoleucine 298	3.7	3.8	3.6	3.9,3.9	3.4	3.6	3.6	3.8	3.5,3.7	3.7
Histidine 299	3.9	3.7	3.7	3.7	3.7	3.8	3.7		3.9	3.3
Valine 302		3.8	3.7	3.8,3.8	3.8,3.8	3.8,4.0	3.6,3.8	3.4,3.7	3.8	3.8
Lysine 305										
Tryptophan 320	3.6		3.3,3.8	3.7,3.8	3.9	3.8	3.7	3.7	3.7,3.9	
Histidine 321	4.0									3.8
Isoleucine 324	3.7	4.0		3.6,3.9				3.8,3.9	4.0	3.4
Tyrosine 328	3.3,3.6	3.8		3.7			3.8	3.8,3.8	3.8,3.8	3.4

**Table 6: Six Other Mitragynine Analog – Active Site Residue Contacts within 4.0  
Angstroms**

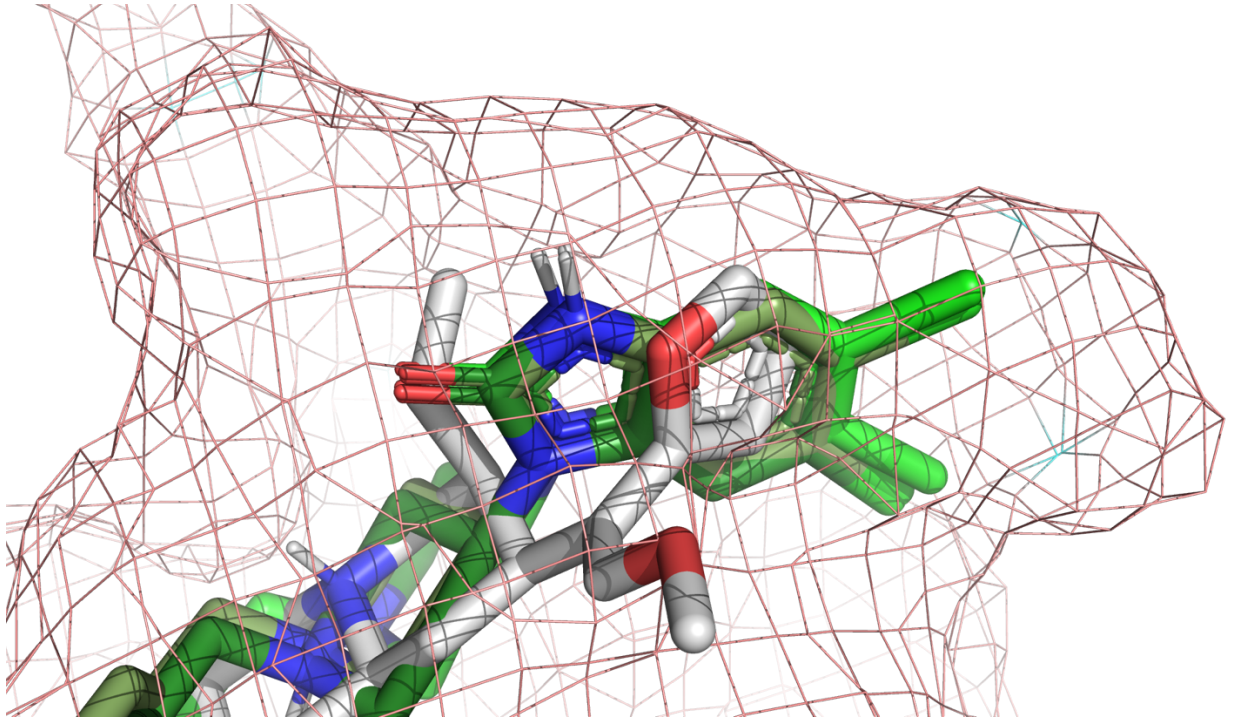
Receptor Residues	Ligand-Receptor Residue Contacts (Angstroms)						
	7-OH-M	R1-25	2-7A	2-7C	2-9A	2-9C	2-21A
Aspartate 56	4	3.7					
Serine 57		3.8	3.5	3	4	3.7	3.5
Glutamine 126	3.5	3.7	3.7	3.7	3.7	3.8,3.9	3.6,3.8,3.9
Tryptophan 135	3.7	3.7		3.5	3.4	3.5,3.9	3.2
Valine 145		3.8	3.4	3.6	3.7	3.3	
Isoleucine 146			3.8	3.7	3.9	3.8	3.8
Aspartate 149	3.2	4.3	3	3.1	2.4	2.4	2.3
Tyrosine 150	3.3		3.5,4.0	2.4,3.1,3.6	3.7,4.0	3.7,3.7,3.8	3.6,3.7
Methionine 153	3.7,4.0		3.8		3.8	3.9	3.6,3.6
Cysteine 219		3.8	3.6		3.7		
Lysine 235	3.8		3.7	4			
Valine 238	3.8	3.8	3.7	3.8	3.6	3.7	3.8
Tryptophan 295	3.8	4			3.3	3.5	3.7
Isoleucine 298	3.7	3.7,3.9	3.8	3.5	3.6	3.4	3.7
Histidine 299	3.9	3.8	3.4	3.6			
Valine 302		3.7,3.8	3.7	3.8,3.9	4	3.9	4
Lysine 305							
Tryptophan 320	3.6	3.8		3.7	3.8		3.6,3.8
Histidine 321	4						
Isoleucine 324	3.7	3.8	3.7		3.7, 3.8	3.8	3.9
Tyrosine 328	3.3,3.6	3.6,4.0	3.4,3.7	4	3.6,3.7,3.7	3.8,3.9	3.7,4.0



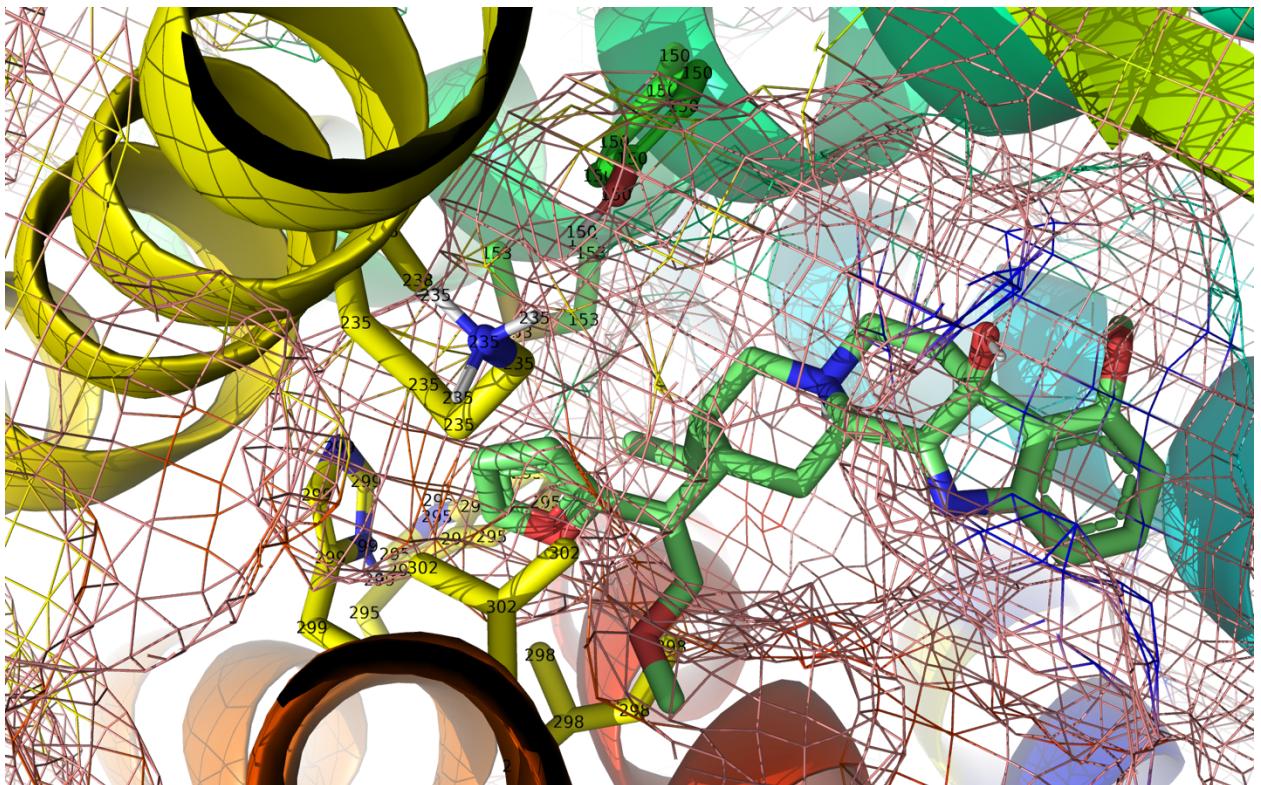
**Figure 23: Binding poses of fifteen successfully screened mitragynine analogs in grid view**



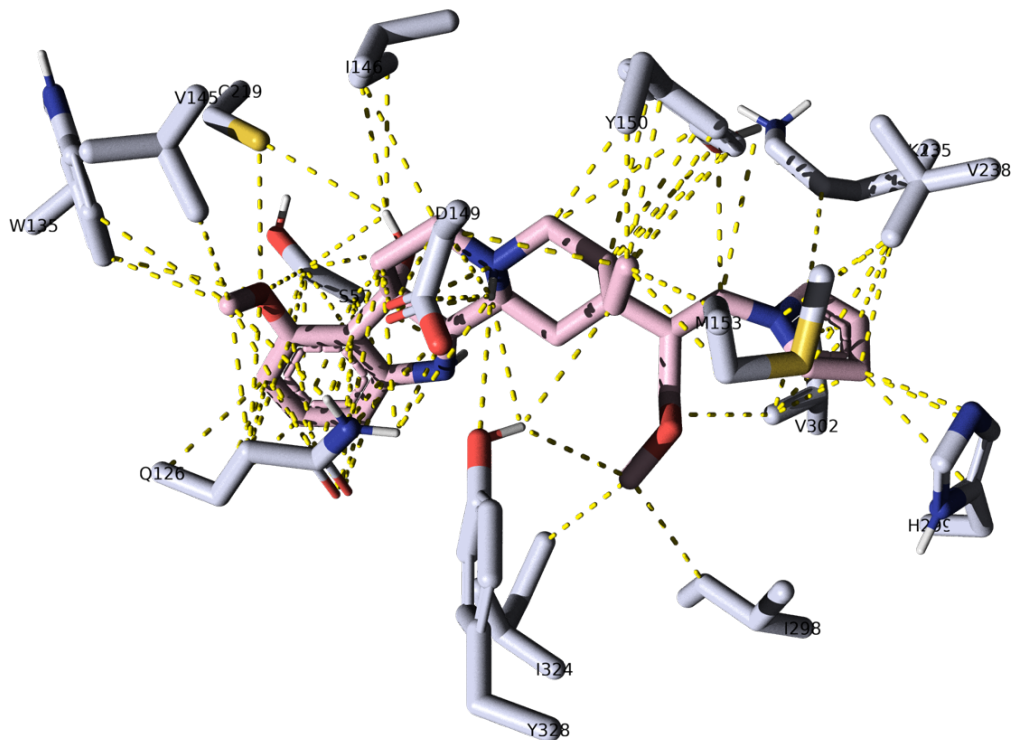
**Figure 24: R1-25 active site residue contacts within 4.0 Å**



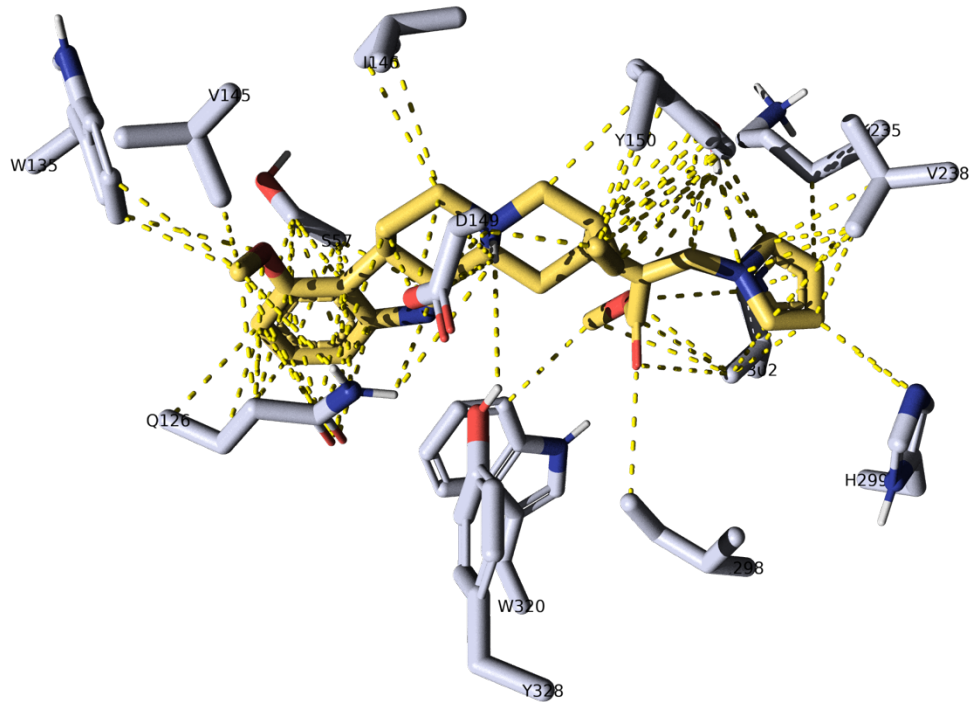
**Figure 25: R1-25 furan group (white) aligned with SR 5,6-dichloro-2H-benzo[d]imidazol-2-one groups (green) in TMH 5&6 binding pocket**



**Figure 26: R1-25 in active site with residues of TMH 5&6 binding pocket**



**Figure 27: 2-7A active site residue contacts within 4.0 Å**



**Figure 28: 2-7C active site residue contacts within 4.0 Å**





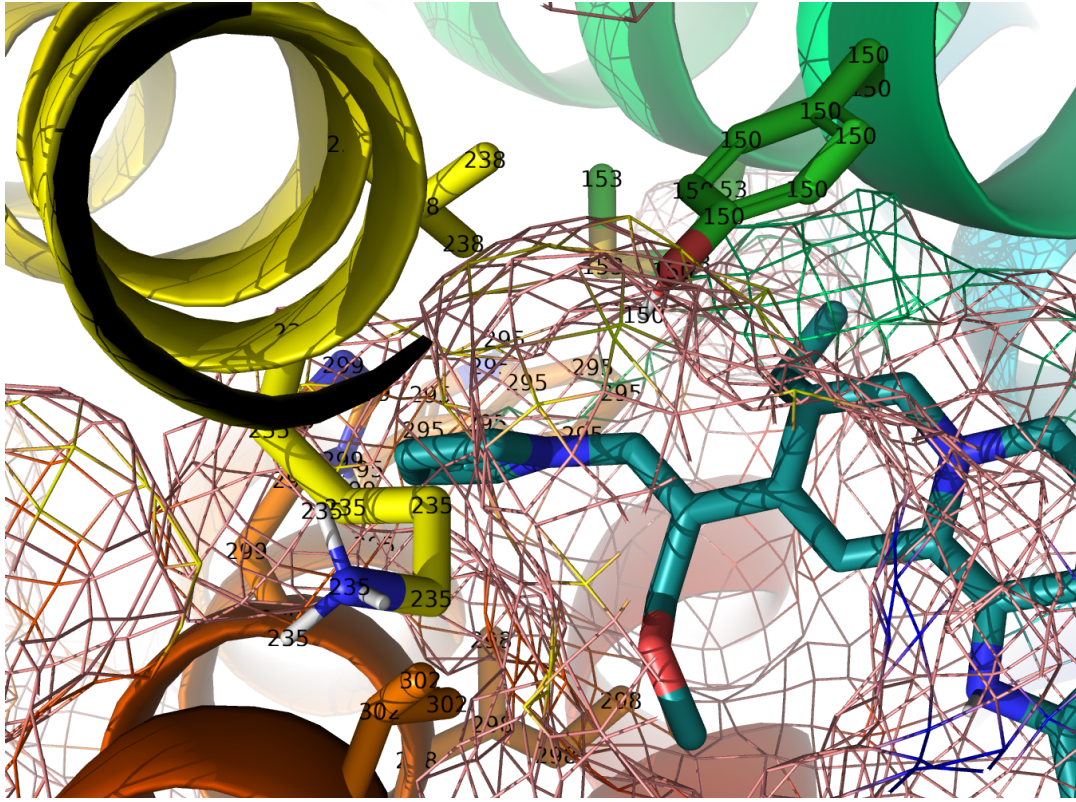


Figure 31: 2-7C in active site with residues of TMH 5&6 binding pocket

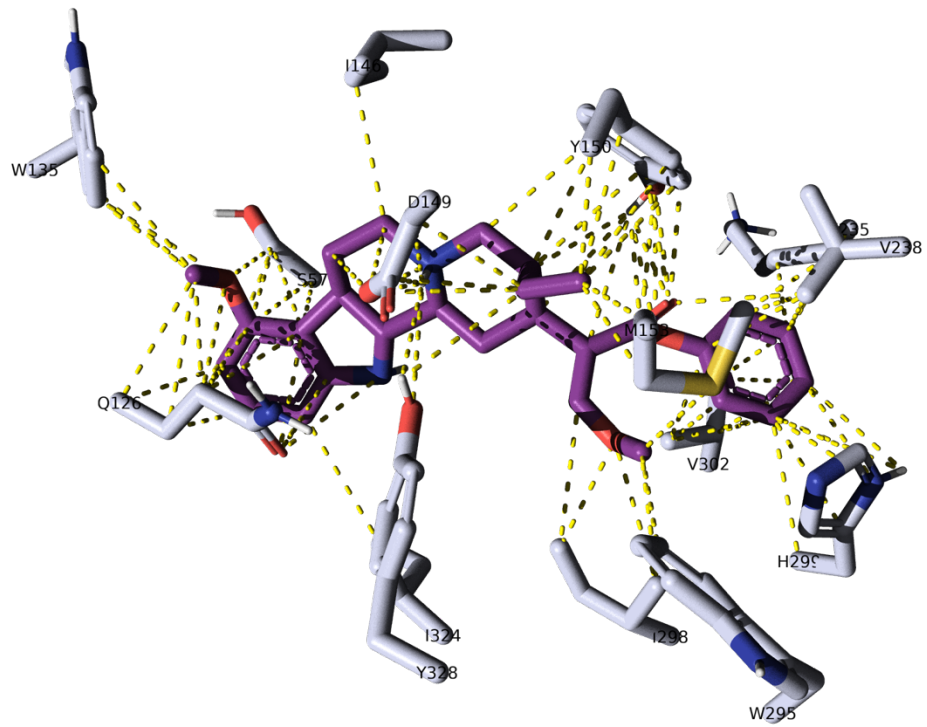
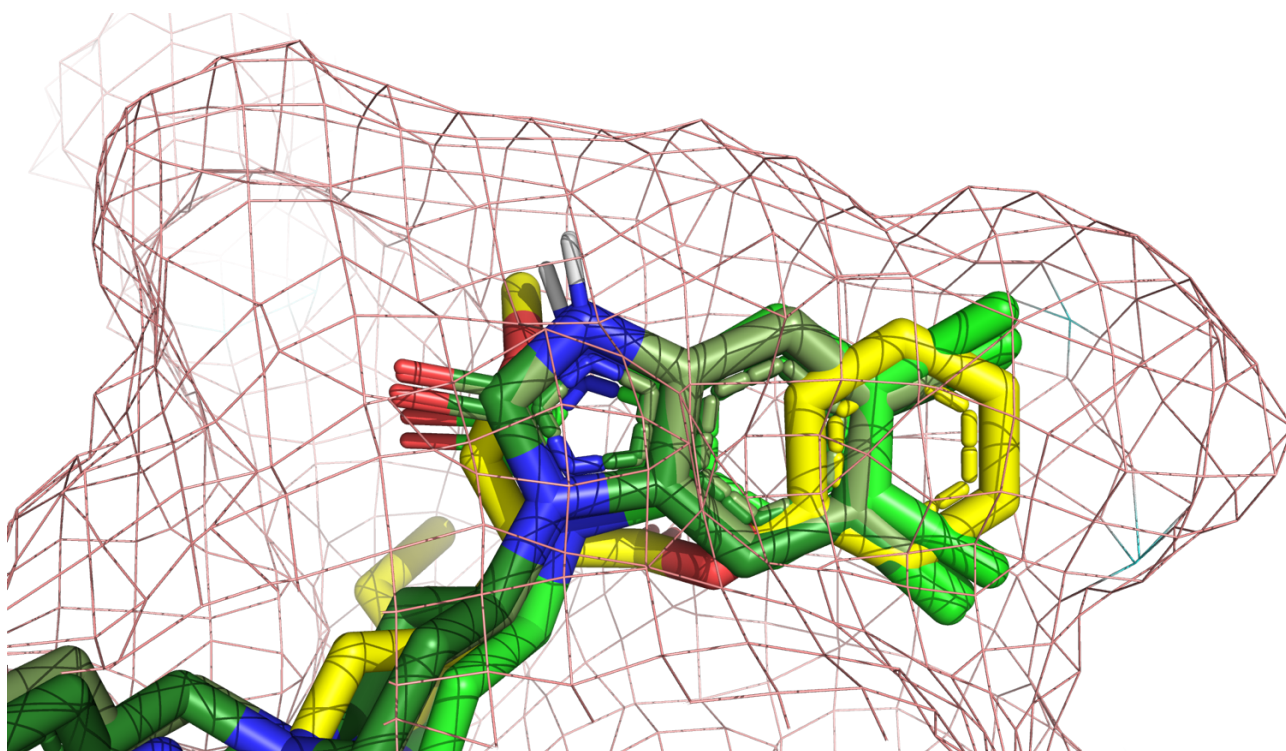
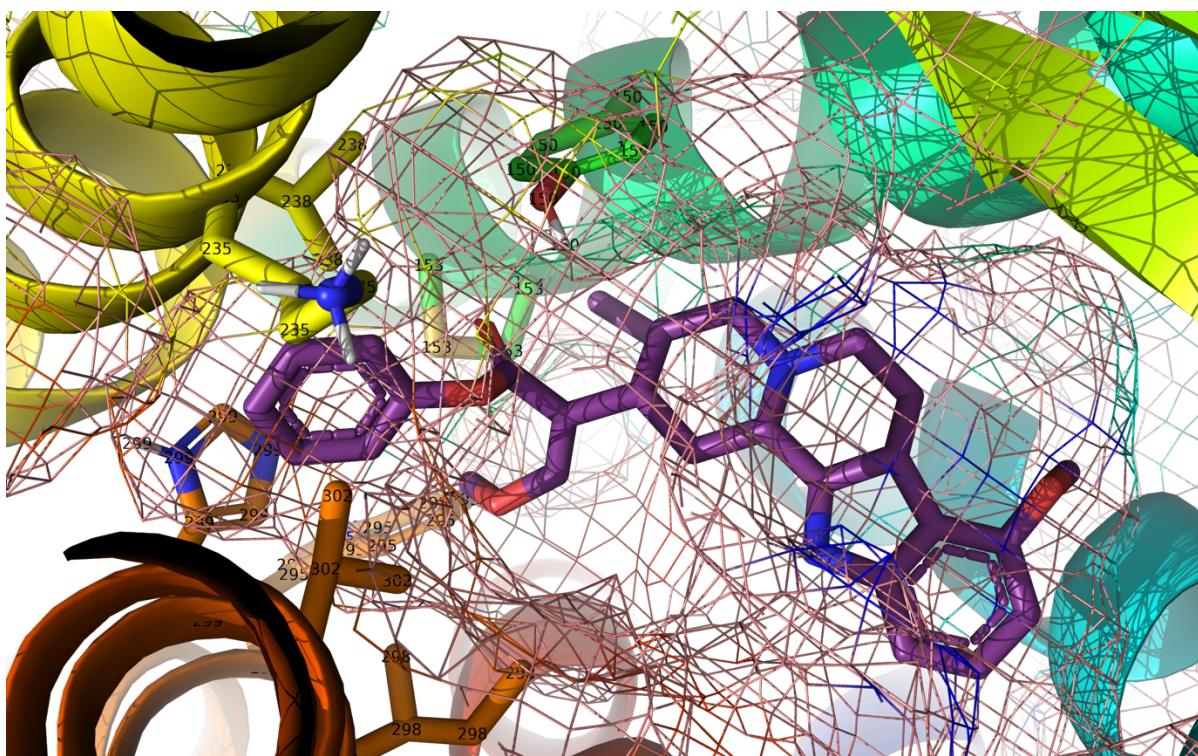


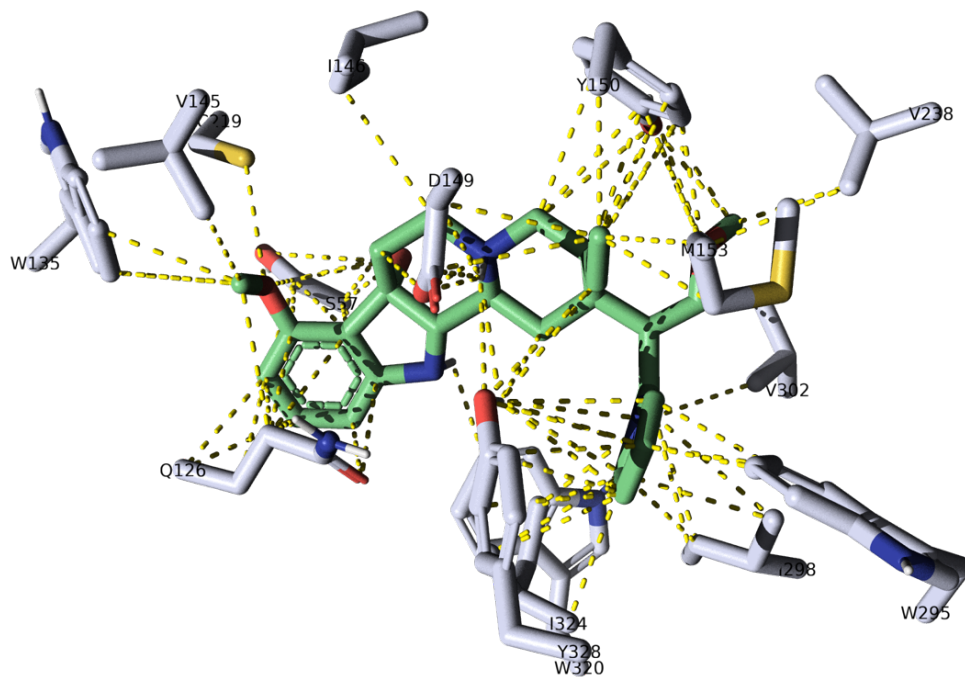
Figure 32: 2-8C active site residue contacts within 4.0 Å



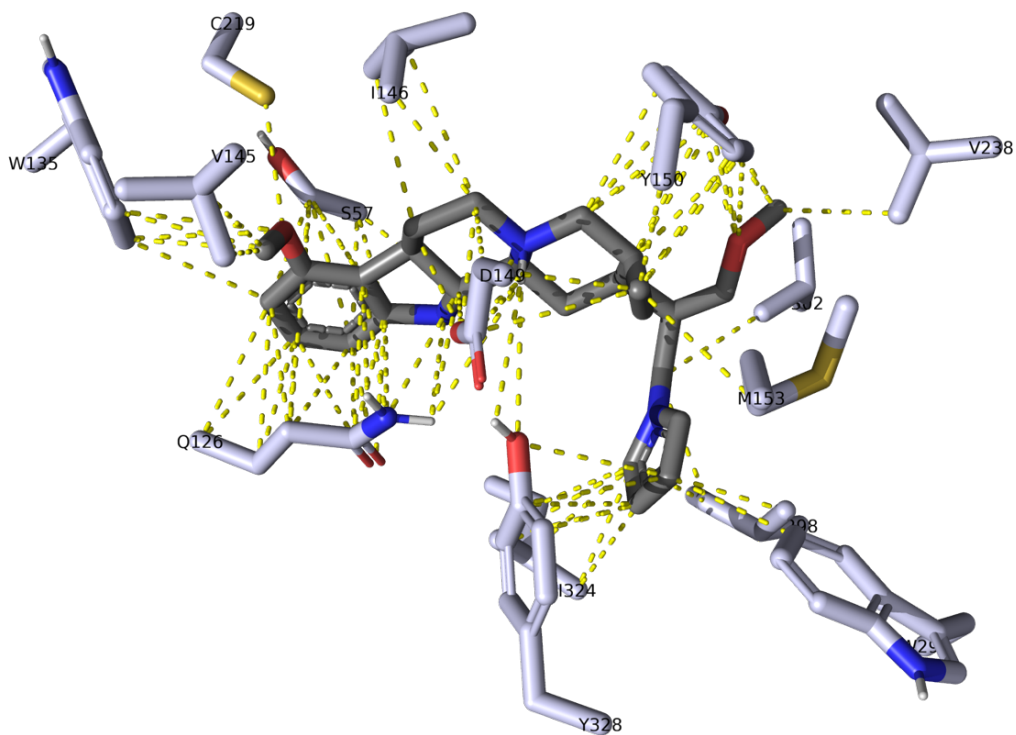
**Figure 33: 2-8C phenyl group (yellow) aligned with SR 5,6-dichloro-2H-benzo[d]imidazol-2-one groups (green) in TMH 5&6 binding pocket**



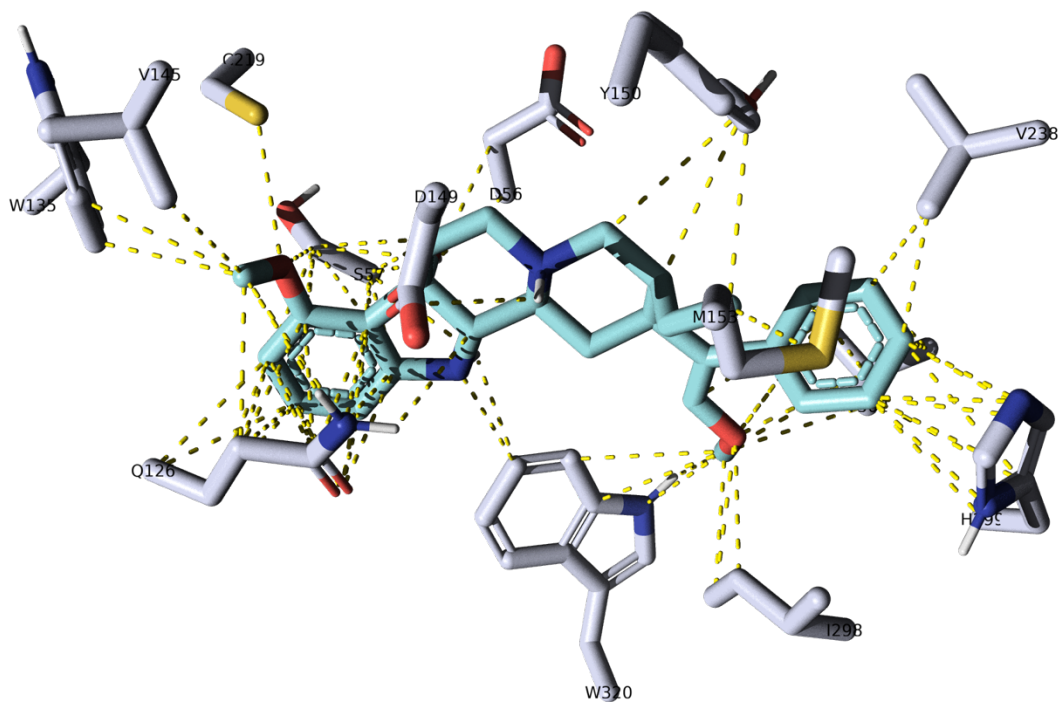
**Figure 34: 2-8C in active site with residues of TMH 5&6 binding pocket**



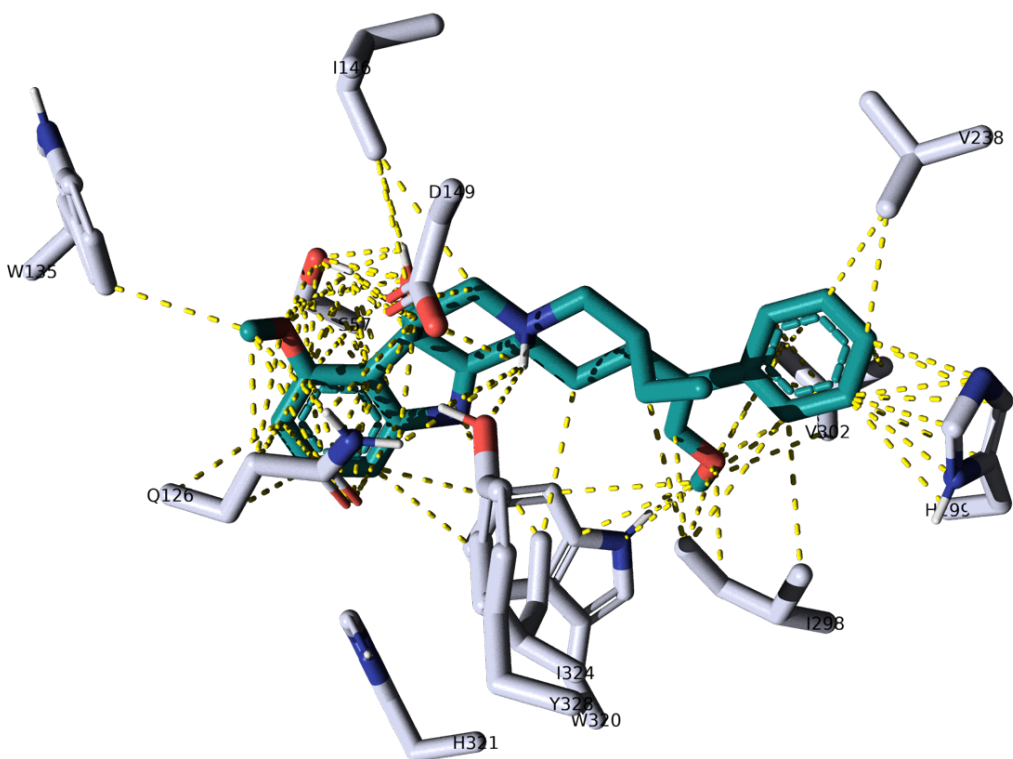
**Figure 35: 2-9A active site residue contacts within 4.0 Å**



**Figure 36: 2-9C active site residue contacts within 4.0 Å**



**Figure 37: 2-15A active site residue contacts within 4.0 Å**



**Figure 38: 2-15B active site residue contacts within 4.0 Å**



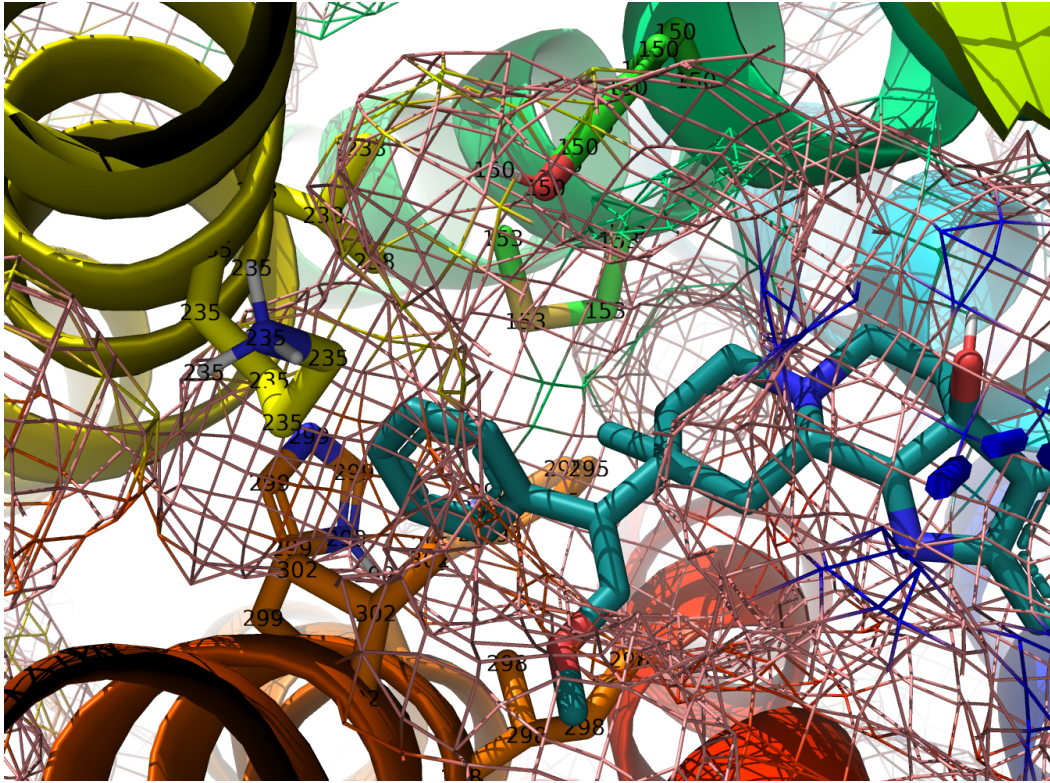


Figure 41: 2-15B in active site with residues of TMH 5&6 binding pocket

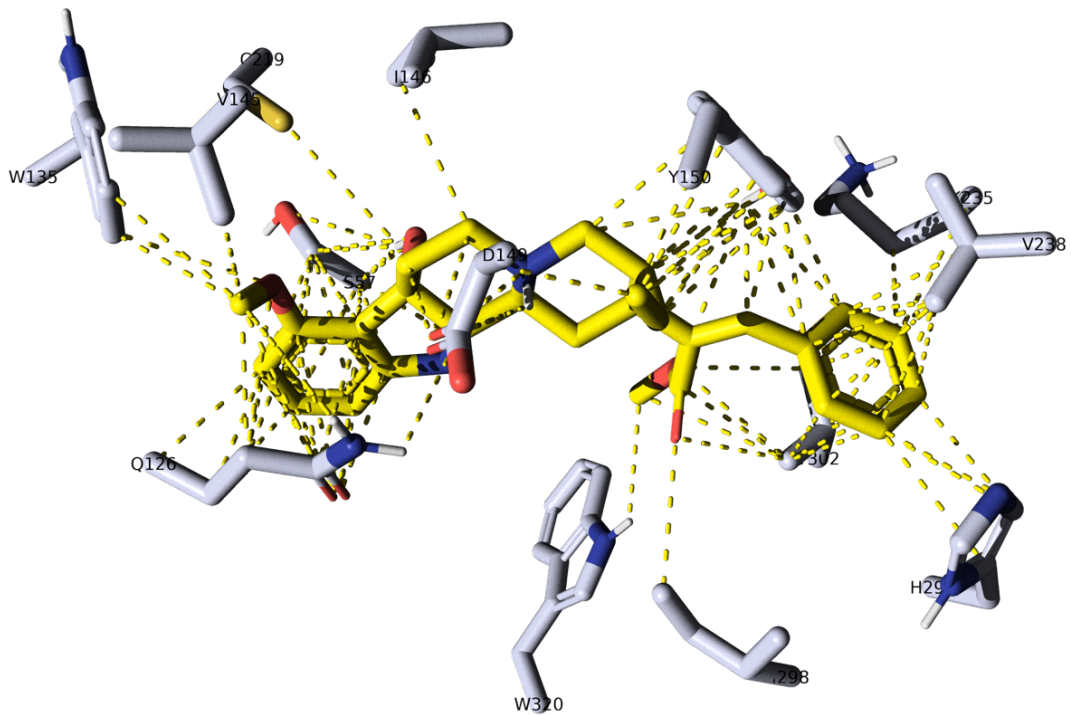
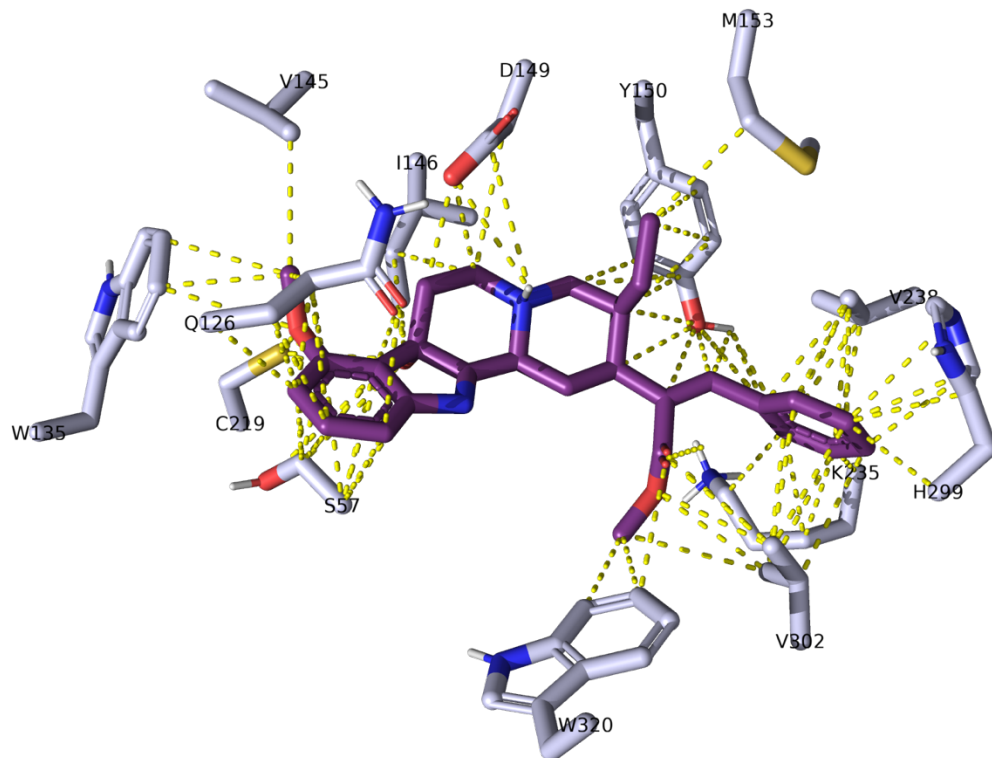
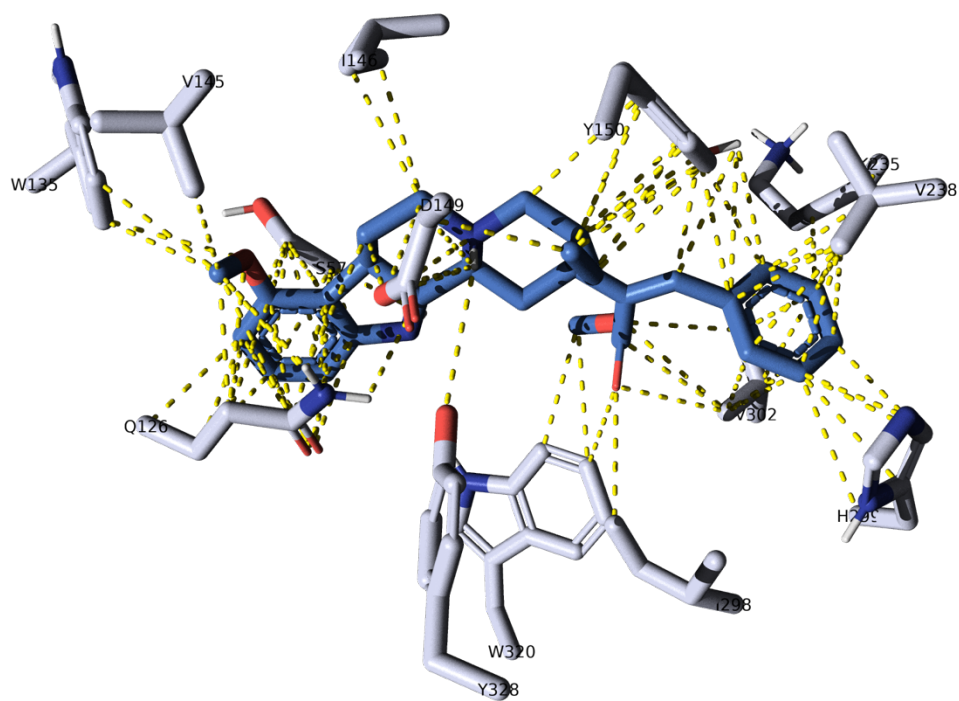


Figure 42: 2-18A active site residue contacts within 4.0 Å

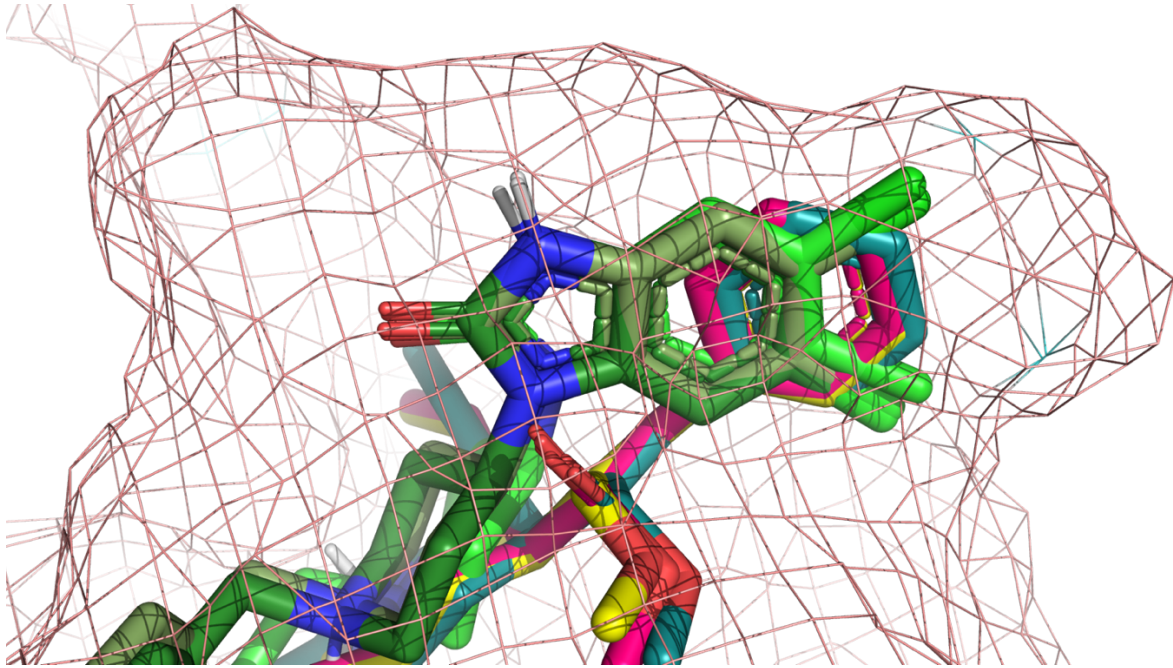


**Figure 43: 2-18B active site residue contacts within 4.0 Å**

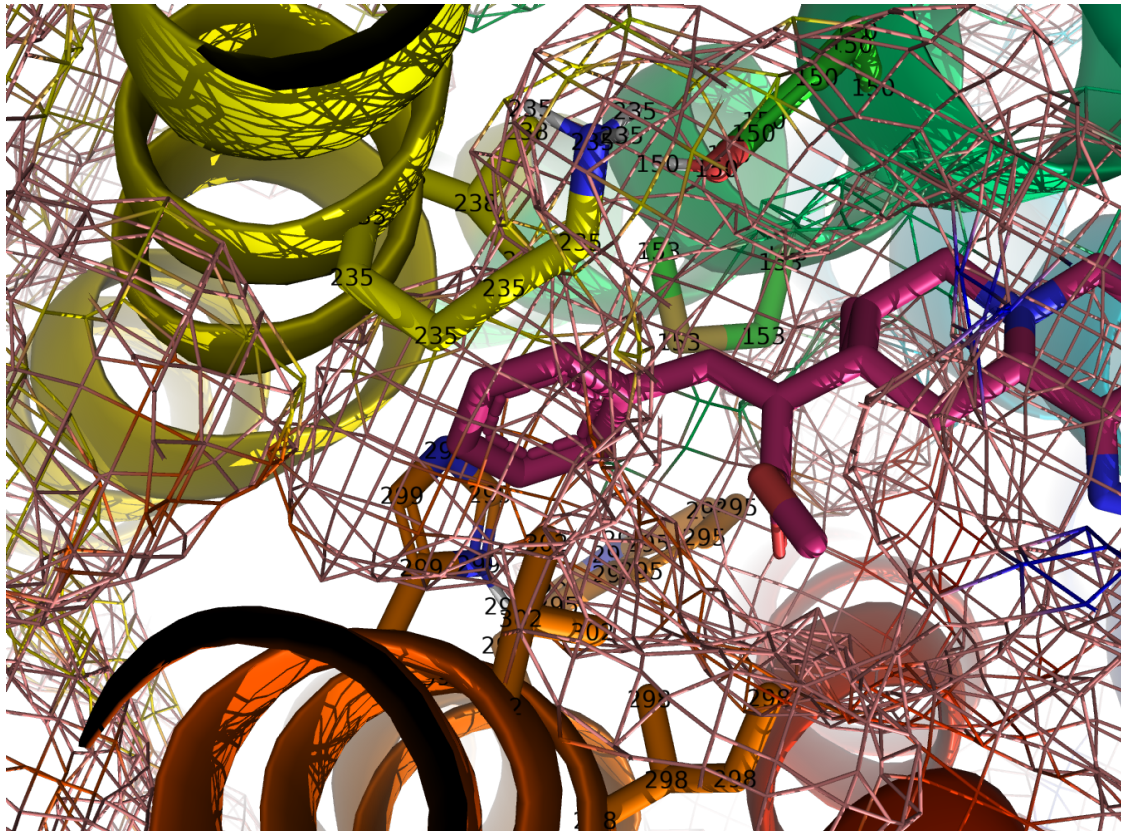


**Figure 44: 2-18C active site residue contacts within 4.0 Å**

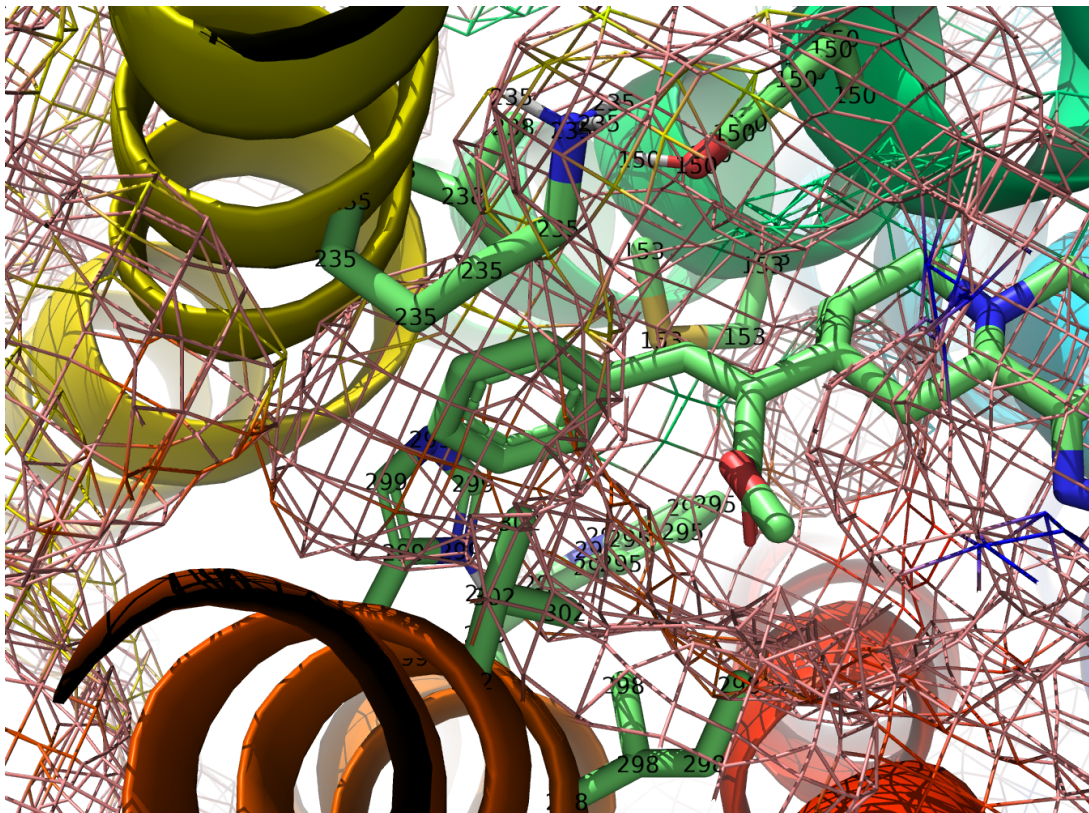




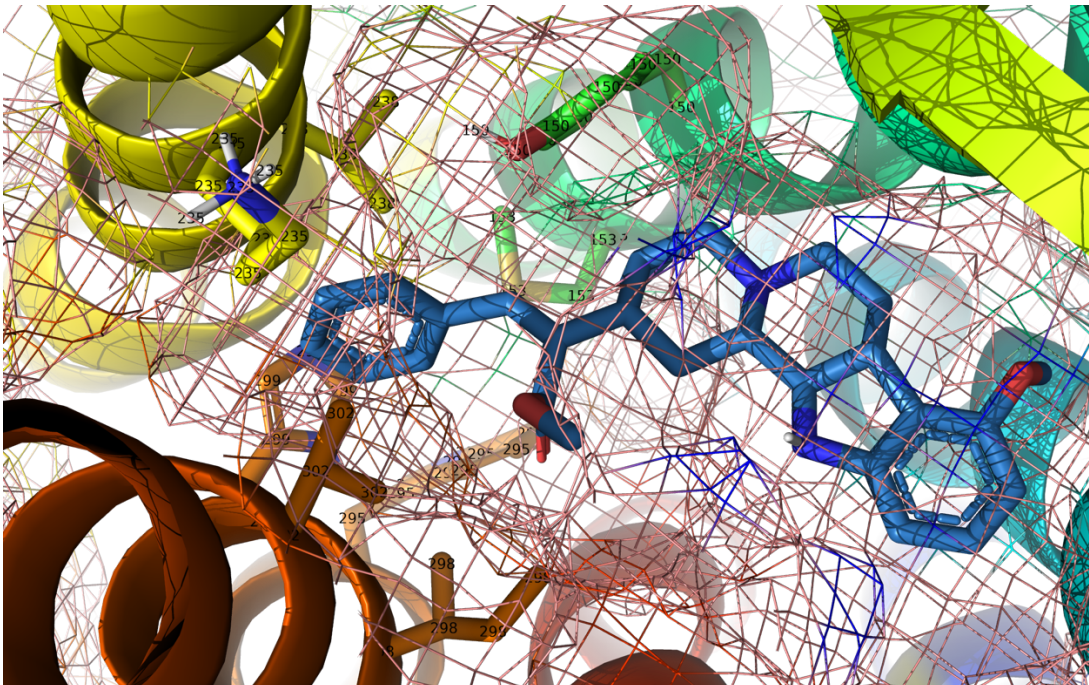
**Figure 45: 2-18A-C phenyl groups (multicolored) aligned with SR 5,6-dichloro-2H-benzo[d]imidazol-2-one groups (green) in TMH 5&6 binding pocket**



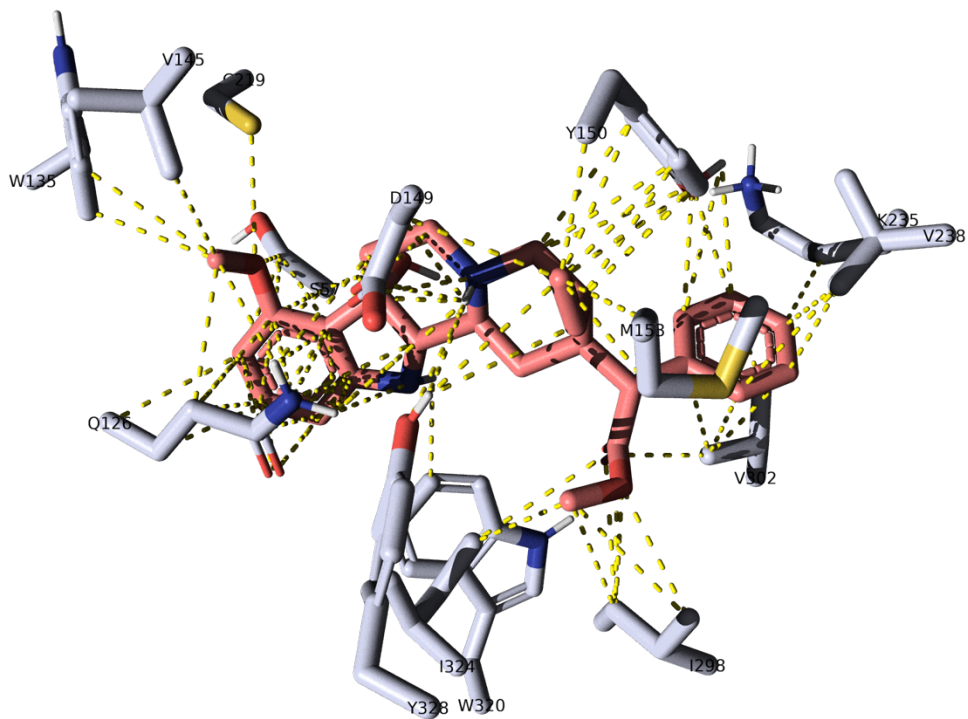
**Figure 46: 2-18A in active site with residues of TMH 5&6 binding pocket**



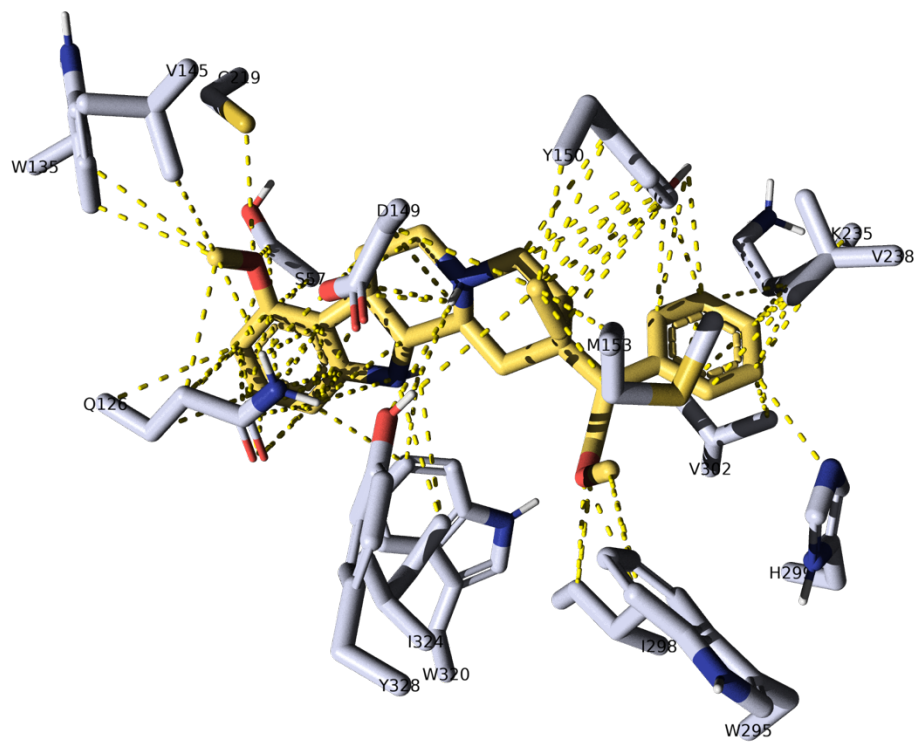
**Figure 47: 2-18B in active site with residues of TMH 5&6 binding pocket**



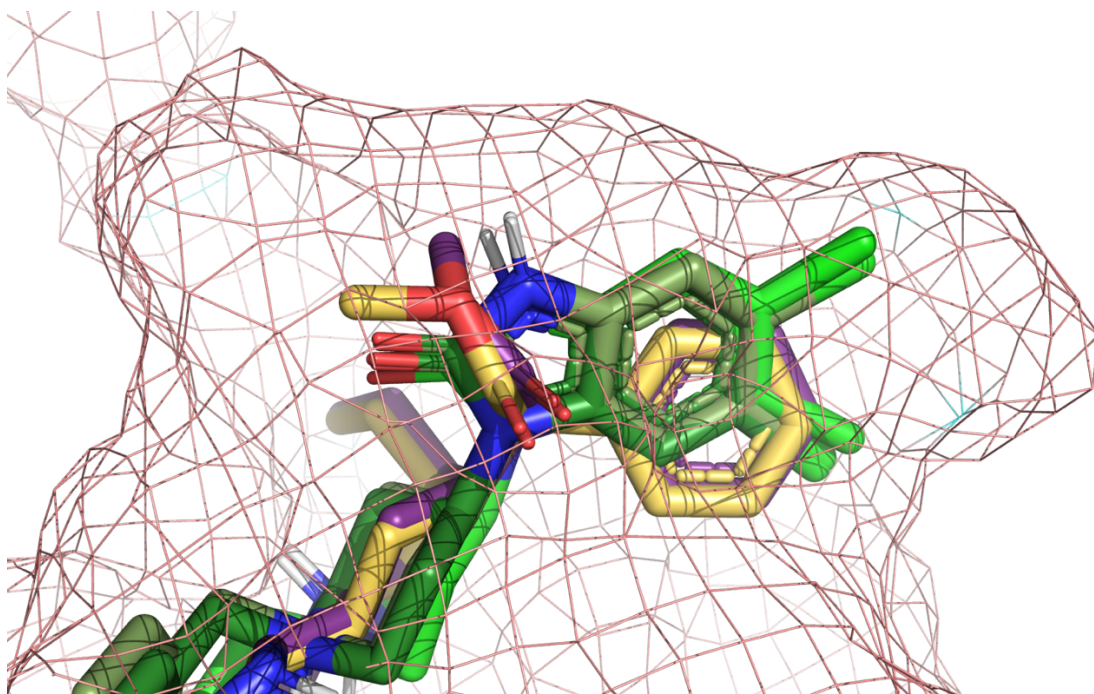
**Figure 48: 2-18C in active site with residues of TMH 5&6 binding pocket**



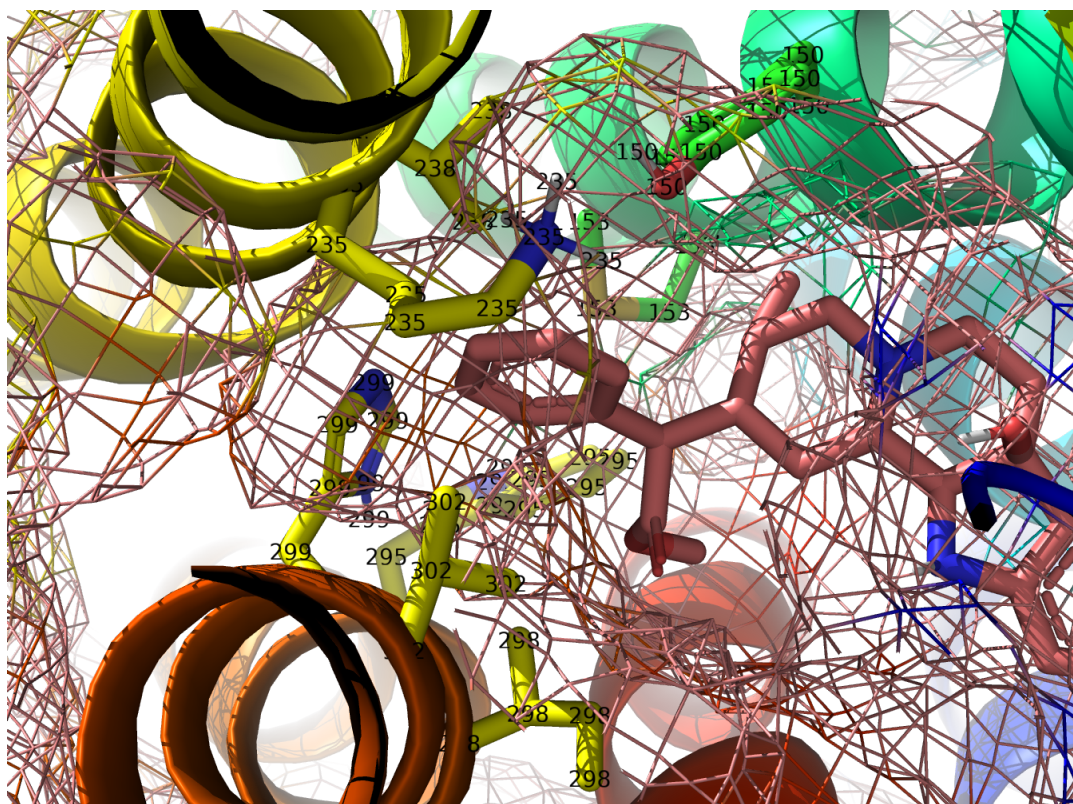
**Figure 49: 2-19A active site residue contacts within 4.0 Å**



**Figure 50: 2-19C active site residue contacts within 4.0 Å**



**Figure 51: 2-19A&C phenyl groups (yellow and purple) aligned with SR 5,6-dichloro-2H-benzo[d]imidazol-2-one groups (green) in TMH 5&6 binding pocket**



**Figure 52: 2-19A in active site with residues of TMH 5&6 binding pocket**

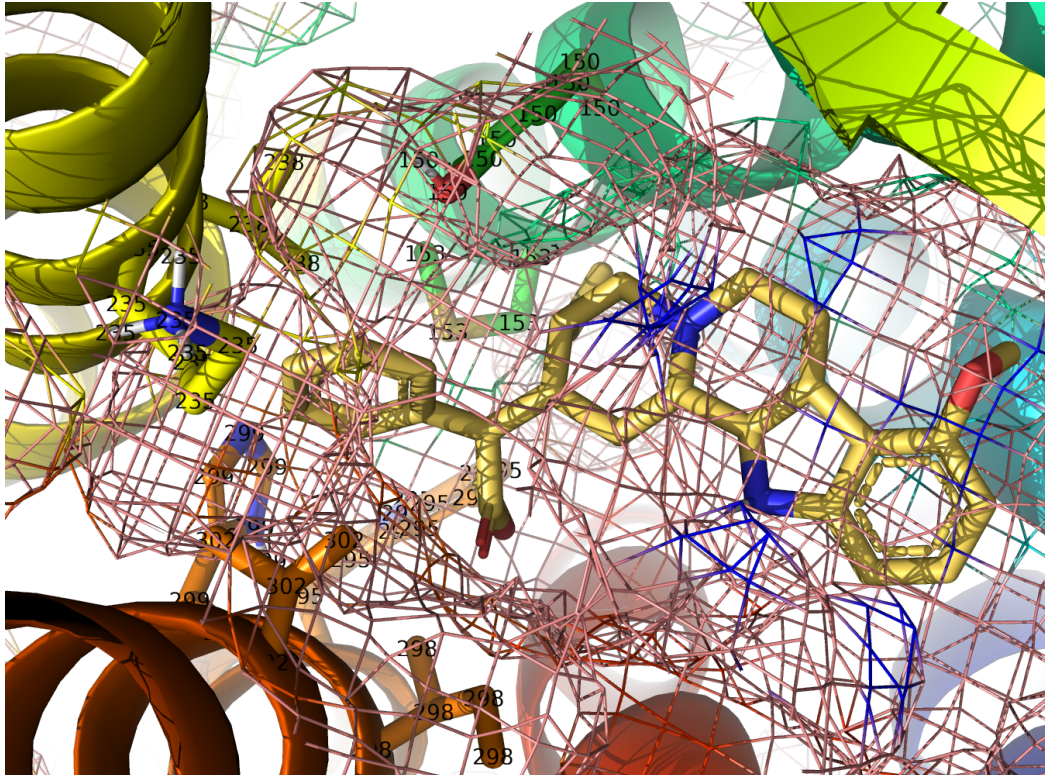


Figure 53: 2-19C in active site with residues of TMH 5&6 binding pocket

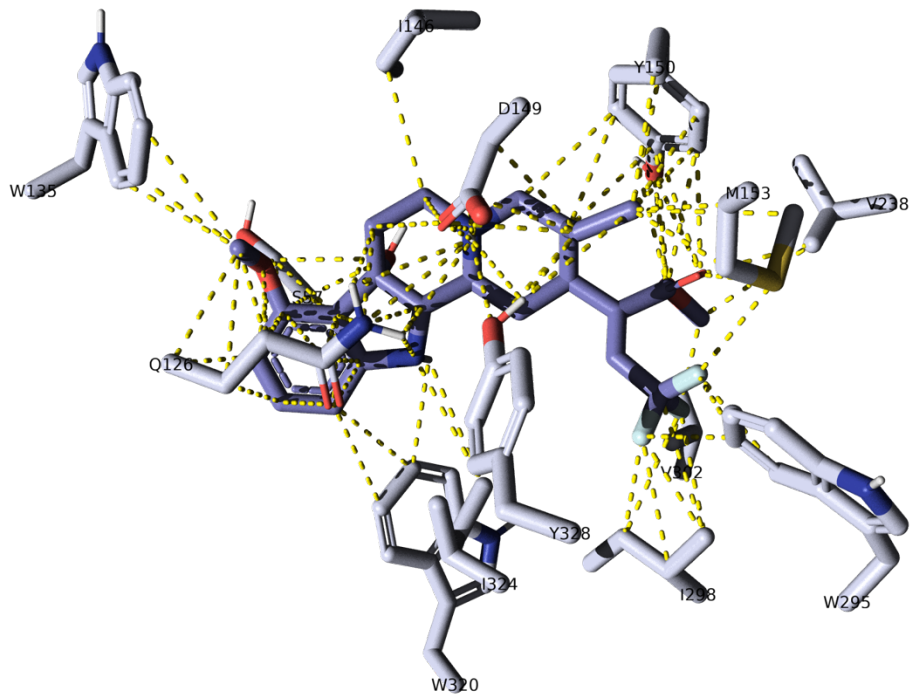
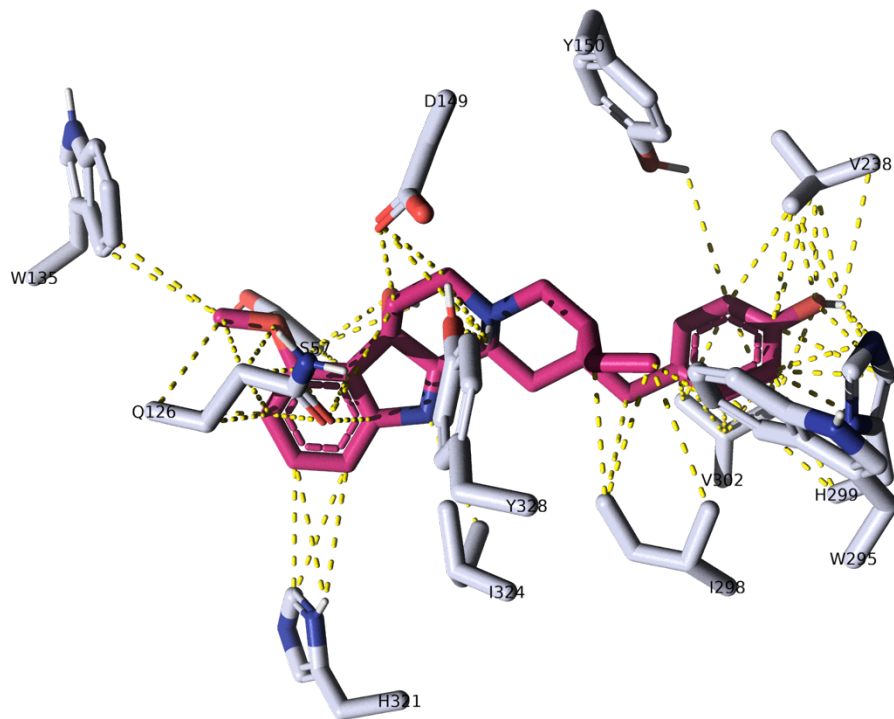
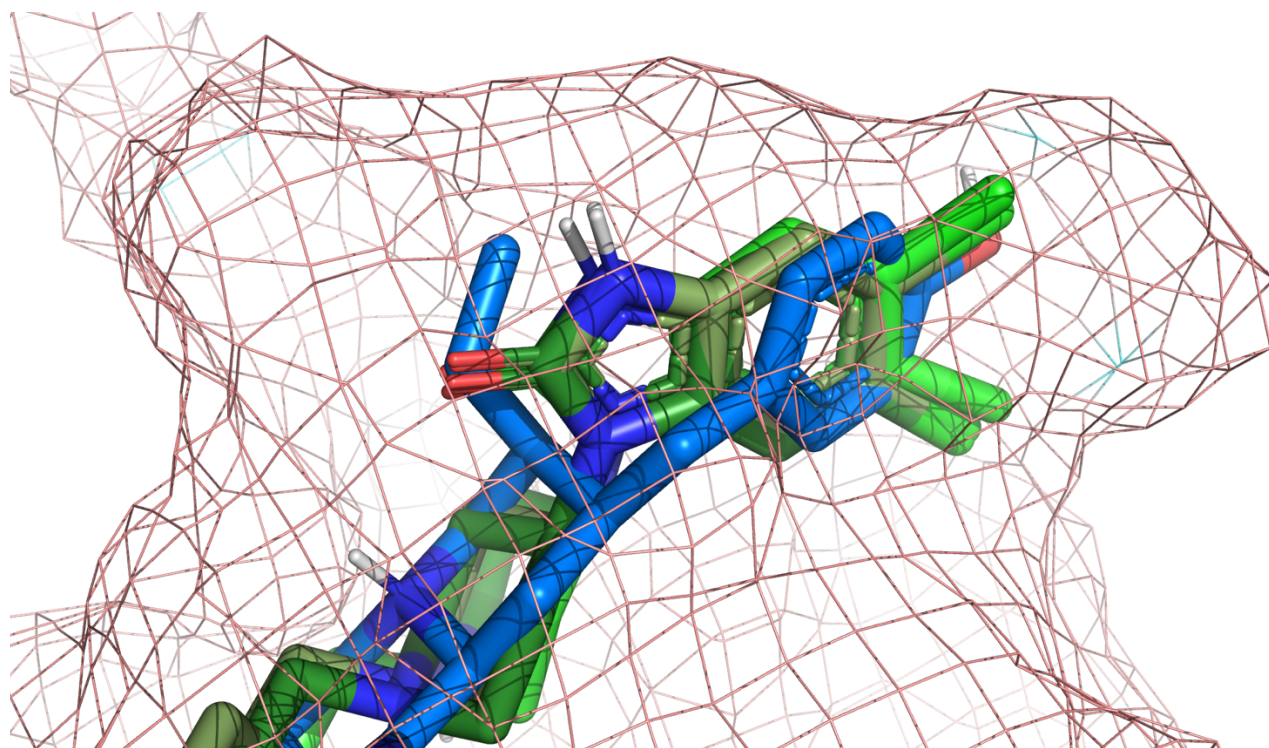


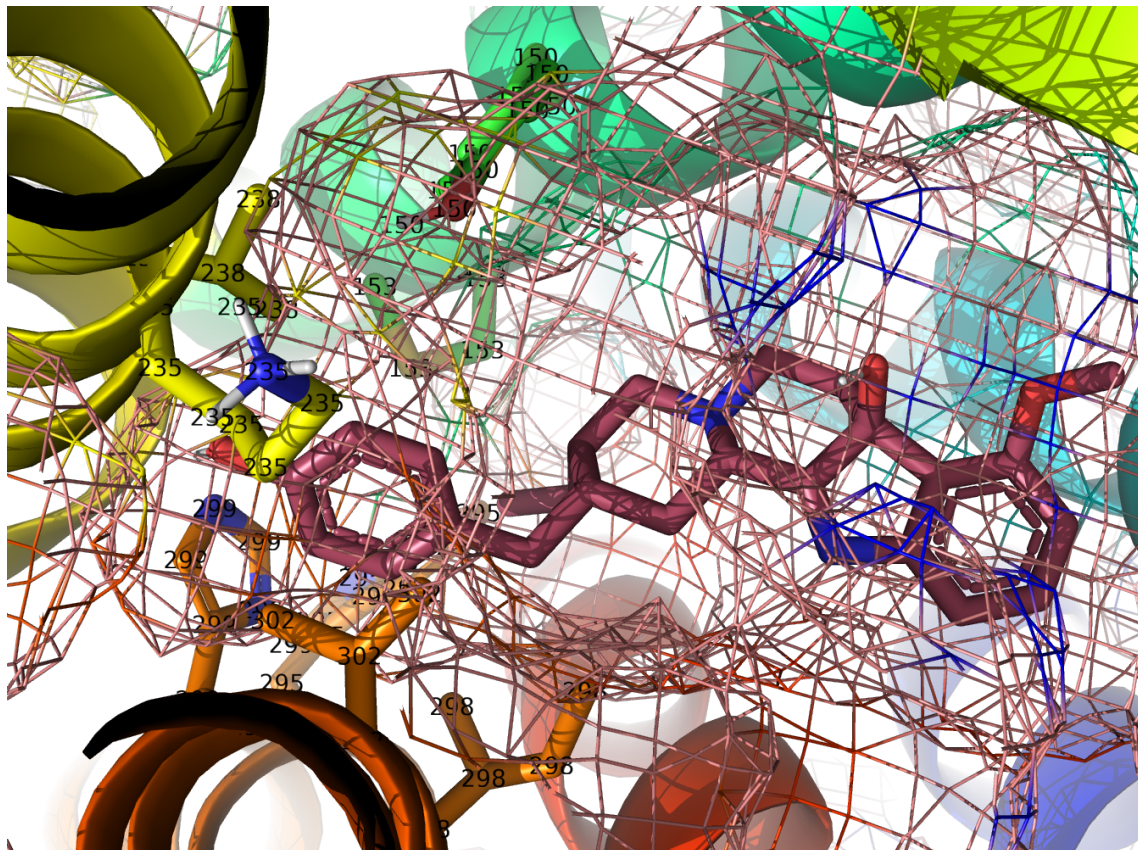
Figure 54: 2-21A active site residue contacts within 4.0 Å



**Figure 55: 2-39E active site residue contacts within 4.0 Å**



**Figure 56: 2-39E phenol group (blue) aligned with SR 5,6-dichloro-2H-benzo[d]imidazol-2-one groups (green) in TMH 5&6 binding pocket**



**Figure 57: 2-39E in active site with residues of TMH 5&6 binding pocket**

In this virtual screen, 185 mitragynine analogs were screened for binding at the mu-opioid receptor. An initial pharmacokinetic screen selecting for GI (gastrointestinal) and BBB (blood-brain-barrier) permeability reduced the initial compound library to 120 analogs. Rigid docking calculations screened by pose and binding affinity reduced the library to twenty analogs. Finally, flexible docking calculations screened by pose and binding affinity reduced the library to fifteen analogs. Screening analog docking results by the flexible docking binding affinity and pose of 7-OH-mitragynine established a high threshold for both rigid and flexible docking results that may have produced false negatives. Still, the fifteen successfully screened molecules contained aromatic or halogenated substitutions to the  $\beta$ -methoxyacrylate and represent a well-defined set of analogs.

Six classes of  $\beta$ -methoxyacrylate substitutions using four aromatic bioisosteres and one halogenated bioisostere are represented in these fifteen molecules (see Table 4). Successful substitution with a pyrrole group was reproduced in four analogs (2-7A&C, and 2-9A&C) and successful substitution with a phenyl group in eight analogs (2-8C, 2-15A&B, 2-18A-C, 2-19A&C). The remaining three analogs represent substitution with furan, phenol, and trifluoromethyl groups in R1-25, 2-39E, and 2-21A, respectively.

From docking calculations, it was evident that binding affinities were significantly lower than 7-OH-mitragynine for all fifteen analogs, with binding affinities ranging from -9.6 kcal/mol to -11.3 kcal/mol (see Table 3). Fourteen of the fifteen final analogs were designed in the second round of drug design where modification to the 9-methoxyindole domain was considered in three ways: (A) 7-OH hydroxyl without an imine resembling MGM biased agonists, (B) 7-OH hydroxyl with an imine to mimic metabolic oxidation at carbon 7, and (C) neither 7-OH hydroxyl nor an imine. Observed binding affinities were not explained by the different classes of these fourteen analogs.

Twelve of the fifteen analogs directed their novel functional group toward the binding pocket of TMH5 and TMH6, analogous to the enol ether of 7-OH-mitragynine. For analogs 2-7A&C, 2-18A-C, and 2-19A&C, some or all of the enol ether was modified while in R1-25, 2-8C, and 2-15A&B modifications were to the methyl ester. 2-39E is the only screened analog where both the enol ether and methyl ester were modified or removed. In the three analogs that directed their modified functional group to the same orientation as the methyl ester of 7-OH-mitragynine, 2-9A&C contained a pyrrole ring in substitute of the methyl ester's O-methyl while 2-21A contained a trifluoromethyl group in substitute of the ether. Interestingly, the pyrrole ring of 2-7 and 2-9 compounds were directed to the analogous group that they substituted in 7-OH-



mitragynine, indicating that the pyrrole group had affinity for the binding sites of both the enol ether and methyl ester of  $\beta$ -methoxyacrylate. Finally, analogs R1-25, 2-8C, and 2-15A&B contained enol ether groups but instead directed their novel functional groups toward TMH5 and TMH6. Follow-up drug design should consider modification of the enol ether with these functional groups while maintaining the methyl ester to better conserve features of the lead compound.

Flexible receptor docking in the 21-residue active site revealed largely conserved residue contacts between 7-OH-mitragynine and the fifteen analogs, a product of binding pose alignment in the virtual screen. Residue contact conservation was greatest for residues such as Gln126, Trp135, Asp149, Tyr150, Val238, Trp302, and Tyr328 of which many have been described in opioid binding (see Table 6) (1,6). All fifteen analogs demonstrated contacts with the adjacent residue Ser57 and two residues showed close contacts with the alkyl side chain of Asp 56. For all Class C analogs of the second round of drug design, no 7-hydroxyl group is present. Many analog contacts with Ser57 were with the alkyl chain of the residue rather than the hydroxyl group itself. Thus, although all analogs showed contacts with Ser57, it was not necessarily indicative of hydrogen bonding between ligand and residue hydroxyl groups and it cannot be concluded that the hydrogen bond network between the 7-hydroxyl group and flexible loop was fully reproducible. Closer inspection revealed that this hydrogen bonding network was maintained, as in 7-OH-mitragynine, only in analogs 2-9A, 2-18A, 2-15B, and 2-18B. However, contact with the residue within 4.0 Å may still indicate the potential for this hydrogen bonding network.

The binding poses of the twelve mitragynine analogs that delivered aromatic functional groups to the binding pocket of TMH5 and TMH6 prompted comparison with the SR biased

agonists which direct a 5,6-dichloro-2H-benzo[d]imidazol-2-one group to the same binding pocket. Existing chemical literature has established that hydrophobic contact with the TMH5 and TMH6 binding pocket and hydrogen-bonding with residue His299 lining the binding pocket is a common feature in opioid binding (1,6). Ligand contact with His299 within 4.0 Å was observed in eleven of these twelve analogs, excluding 2-19A. The three analogs that delivered a modified group to the same position as the methyl ester of 7-OH-mitragynine did not show close contacts with His299.  $\pi$ -stacking between His299 and the aromatic groups bound to this pocket may explain the activity of SR agonists and the success of many screened mitragynine analogs with aromatic functional groups directed to this receptor pocket. AutoDock Vina's scoring function has been reported to treat  $\pi$ - $\pi$  interactions with "sufficient specificity" that these interactions were treated properly when docking mitragynine analogs and SR agonists (22). Modeled  $\pi$ - $\pi$  stacking in docking calculations may partly explain the significantly improved binding affinity of mitragynine analogs compared to 7-OH-mitragynine which does not deliver any aromatic group to the binding pocket between TMH5 and TMH6 .

Overlap of binding poses for the SR biased agonists with these twelve analogs revealed similar orientation and location within the binding pocket, particularly for residues with phenyl/phenol substituents such as 2-8C, 2-15A&B, 2-18A-C, 2-19A&C, and 2-39E. The presence of two chlorine substituents in SR agonists may explain the accommodation of the pyrrole and furan groups to this binding pocket in 2-7A&C and R1-25, respectively. Additionally, alignments suggest that the binding pocket may accommodate substituted phenyl groups delivered by the mitragynine scaffold. This may prove to be a fruitful direction of opioid agonist discovery, as hydrogen bonding capability of aromatic groups in this binding pocket may enable greater affinity without compromising BBB permeability. Aromatic systems can function

as weak hydrogen bond acceptors for NH/ $\pi$  interactions and electron-donating substituents to aromatic rings have been associated with greater hydrogen bonding strength of the aromatic system (23,24). In contrast to the electron withdrawing chlorine substituents of SR agonists, future drug design of mitragynine analogs may consider expansion of the phenyl, pyrrole, and furan groups with the addition of electron-donating substituents. This drug design strategy may accomplish the challenge of target accessibility while also preserving essential interactions with active site residues, in particular  $\pi$ -stacking and NH/ $\pi$  hydrogen bonding with His299 of the TMH5 and TMH6 binding pocket.

## **V. Conclusions**

The realization that opioid agonists can differentially activate G-protein and  $\beta$ -arrestin signaling has informed an active field of drug design for the development of biased agonists that may provide improved classes of pharmaceuticals for pain-relief (4). Mitragynine is a useful lead compound in drug design for its activity at the MOR as a biased partial agonist. The recent synthesis and study of SR compounds is a milestone in the design and testing of biased agonists (8). Comparing the binding of three related mitragynine compounds and three biased SR compounds clarified structure-activity relationships for these agonists and also informed the rational design of mitragynine analogues. A virtual screen involving a pharmacokinetics filter and two rounds of molecular docking revealed fifteen successfully screened analogs from an initial compound library of 185 analogs. The high threshold of the docking screen may have reduced the findings of this study by producing false negatives. Successfully screened analogs primarily had aromatic substitutions to the  $\beta$ -methoxyacrylate group and directed them toward a binding pocket between TMH5 and TMH6. This resembled the 5,6-dichloro-2H-

benzo[d]imidazol-2-one functional group pose in SR agonist docking. The findings of the present study refine the design of mitragynine analogs and expand upon the possible activity of the lead compound 7-OH-mitragynine in the mu-opioid receptor. Although bias cannot be inferred from virtual screening alone, the mitragynine scaffold demonstrates potential as a novel structure to deliver biased activation at the mu-opioid receptor.

## VI. References

1. “Docking and Pharmacophore Modeling of Biased Mu-Opioid Receptor Agonists to Guide Mitragynine Analogue Design”, James Fanning, Chemistry 5440 Project 2, Fall 2019, Professor Richard Spinney, Ph.D., The Ohio State University, 3 December 2019
2. “Molecular Basis of Opioid Action: From Structures to New Leads,” Manglik, Aashish, *Biological Psychiatry*, Volume 87, Issue 1, 6 – 14
3. “Structural Determinants for the Binding of Morphinan Agonists to the  $\mu$ -Opioid Receptor,” Cong X, Campomanes P, Kless A, Schapitz I, Wagener M, et al, (2015) PLOS ONE 10(8): e0135998, <https://doi.org/10.1371/journal.pone.0135998>
4. “Arresting the Development of Addiction: The Role of B-Arrestin 2 in Drug Abuse,” Kirsten A. Porter-Stransky and David Weinshenker, *Journal of Pharmacology and Experimental Therapeutics*, June 1, 2017, 361 (3) 341-348, <https://doi.org/10.1124/jpet.117.240622>
5. “7-Hydroxymitragynine Is an Active Metabolite of Mitragynine and a Key Mediator of Its Analgesic Effects,” Andrew C. Kruegel, et al, *ACS Cent. Sci.* 2019, 5, 6, 992-1001 Publication Date: May 29, 2019 <https://doi.org/10.1021/acscentsci.9b00141>
6. “Synthetic and Receptor Signaling Explorations of the Mitragyna Alkaloids: Mitragynine as an Atypical Molecular Framework for Opioid Receptor Modulators,” Andrew C Kruegel, et al, *Journal of the American Chemical Society* vol. 138,21 (2016): 6754-64. doi:10.1021/jacs.6b00360
7. “MGM-16, a Novel Dual-Acting  $\mu$ - and  $\delta$ -Opioid Agonist,” Kenjiro Matsumoto, et al, *Journal of Pharmacology and Experimental Therapeutics* March 1, 2014, 348 (3) 383-392; DOI: <https://doi.org/10.1124/jpet.113.20810>
8. “Bias Factor and Therapeutic Window Correlate to Predict Safer Opioid Analgesics,” CL Schmid, et al, *Cell*. 2017;171(5):1165–1175.e13. doi:10.1016/j.cell.2017.10.035
9. “SWISS-MODEL: homology modelling of protein structures and complexes,” A., Bertoni, et al, SWISS-MODEL Workspace/GMQE Waterhouse, *Nucleic Acids Res.* 46, W296-W303 (2018).
10. NIH NP\_001008503.2 mu-type opioid receptor isoform MOR-1O [Homo sapiens]
11. “Structural insights into  $\mu$ -opioid receptor activation,” W. Huang, et al, *Nature* 524, 315–321 (2015). <https://doi.org/10.1038/nature14886>
12. “YASARA View – molecular graphics for all devices – from smartphones to workstations,” Krieger E1 and G. Vriend, *Bioinformatics*. 2014.
13. Molecular Operating Environment (MOE); Chemical Computing Group Inc.: Montreal, QC, Canada, 2016.
14. "UCSF Chimera - A Visualization System for Exploratory Research and Analysis," E.F. Pettersen, et al, *Journal of Computational Chemistry* 2004, 25(13):1605-1612
15. “Autodock4 and AutoDockTools4: automated docking with selective receptor flexibility,” Morris, G. M., Huey, R., Lindstrom, W., Sanner, M. F., Belew, R. K., Goodsell, D. S. and Olson, A. J, *Journal of Computational Chemistry* 2009, 16: 2785-91
16. “New Developments in Molecular Orbital Theory,” C. C. J. Roothaan, *Rev. Mod. Phys.*, 23 (1951) 69. DOI: 10.1103/RevModPhys.23.69.
17. Spartan'16 Wavefunction Inc., Irvine, CA
18. “AutoDock Vina: improving the speed and accuracy of docking with a new scoring function, efficient optimization and multithreading,” O. Trott and A. J. Olson, *Journal of Computational Chemistry* 31 (2010) 455-461, DOI 10.1002/jcc.21334

19. PyMOL, DeLano, W.L. (2002), DeLano Scientific, San Carlos, CA, 700
20. "The Practice of Medicinal Chemistry (Third Edition)," Editor(s): Camille Georges Wermuth, et al, *Academic Press*, 2008. Print.
21. "SwissADME: a free web tool to evaluate pharmacokinetics, drug-likeness and medicinal chemistry friendliness of small molecules," A. Daina, et al, *Sci Rep.* 2017;7:42717. Published 2017 Mar 3. doi:10.1038/srep4271722
22. "Aromatic interactions at the ligand–protein interface: Implications for the development of docking scoring functions," M. Brylinski, *Chem Biol Drug Design* 2018; 91: 380-390 <https://doi.org/10.1111/cbdd.13084>
23. "π-Hydrogen bonding and aromaticity: A systematic interplay study," Nekoei, A-Reza & Vatanparast, Morteza. (2018), *Physical Chemistry Chemical Physics*. 21. 10.1039/C8CP07003B.
24. "A molecular interaction field describing nonconventional intermolecular interactions and its application to protein–ligand interaction prediction," Daichi Hayakawa, Nahoko Sawada, Yurie Watanabe, Hiroaki Gouda, *Journal of Molecular Graphics and Modelling*, Volume 96, 2020, 107515, ISSN 1093-3263, <https://doi.org/10.1016/j.jmgm.2019>.